



# The ACCESS-AM2 climate model strongly underestimates aerosol concentration in the Southern Ocean, but improving it could be problematic for the modelled climate system

Sonya L. Fiddes<sup>1</sup>, Matthew T. Woodhouse<sup>2,1</sup>, Marc D. Mallet<sup>1</sup>, Liam J. Lamprey<sup>1</sup>, Ruhi S. Humphries<sup>2,1</sup>, Alain Protat<sup>3,1</sup>, Simon P. Alexander<sup>4,1</sup>, Hakase Hayashida<sup>5</sup>, Samuel Putland<sup>6</sup>, Branka Miljevic<sup>6</sup>, and Robyn Schofield<sup>7</sup>

<sup>1</sup>Australian Antarctic Program Partnership, Institute for Marine and Antarctic Studies, University of Tasmania, Hobart, Australia

<sup>2</sup>CSIRO Environment, Melbourne, Australia

<sup>3</sup>Bureau of Meteorology, Melbourne, Australia

<sup>4</sup>Australian Antarctic Division, Hobart, Australia

<sup>5</sup>Application Laboratory, Japan Agency for Marine-Earth Science and Technology, Yokohama, Japan

<sup>6</sup>School of Earth and Atmospheric Sciences, Queensland University of Technology, Brisbane, Queensland, Australia

<sup>7</sup>School of Geography, Earth and Atmospheric Sciences, University of Melbourne, Melbourne, Victoria, Australia

**Correspondence:** Sonya Fiddes (sonya.fiddes@utas.edu.au)

## Abstract.

The interaction of natural marine aerosol with clouds and radiation is a significant source of climate model uncertainty. The Southern Ocean represents a key area to understand these interactions, and a region where significant model biases exist. Here we provide an evaluation of the Australian Community Climate and Earth System Simulator atmosphere model which includes a double-moment aerosol scheme. We evaluate against condensation nuclei (N10) and cloud condensation nuclei (CCN) from seven ship campaigns and three terrestrial locations, spanning the years 2015-2019. We find that N10 is heavily underestimated in the model across all regions and seasons by more than 50% and in some cases by over 80% at higher latitudes. CCN is also strongly underestimated over marine and Antarctic regions, often by more than 50%. We then perform seven sensitivity tests to explore different aerosol configurations. We find that updating the dimethyl sulfide climatology and turning on the primary marine organic aerosol flux marginally improves marine CCN by between 4-9%. N10 however was reduced by between 3-9%, resulting in worse model performance. The Southern Ocean radiative bias is also reduced by this combination of changes, with limited adverse effects. We also test altering the sea spray flux to use wind gust instead of mean wind speed, which significantly improved CCN in the marine regions, but resulted in detrimental impacts on the radiation budget. Our results indicate significant problems in the model's microphysical processes and with over tuning. We suggest this needs to be addressed in a holistic way.

## 1 Plain Language Summary

The interaction between natural marine aerosols, clouds and radiation in the Southern Ocean is a major source of uncertainty in climate models. We evaluate the Australian climate model using aerosol observations and find it underestimates aerosol

number often by over 50%. Model changes were tested to improve aerosol concentrations, but some of our changes had severe negative effects on the larger climate system, highlighting issues in aerosol-cloud interaction modelling.

## 20 **2 Introduction**

Atmospheric aerosol have an important effect on radiation, cloud and precipitation processes that make them an influential component of the Earth's climate. Aerosol affect the Earth's energy budget directly by scattering and absorbing incoming solar radiation, resulting in a cooling effect (McCormick and Ludwig, 1967). Aerosol can also affect the Earth's energy budget indirectly by acting as cloud condensation nuclei (CCN) which enable cloud droplet formation and influence the clouds reflectivity (albedo) and absorption of radiation (Twomey, 1974; Albrecht, 1989; Pincus and Baker, 1994). The ocean surface acts as an important source of natural aerosol to the atmosphere, producing sea spray aerosol (SSA) which is made up by both primary marine organic (PMO) aerosol and sea salts, as well as secondary aerosols derived from the oxidation of dimethyl sulfide (DMS).

Aerosol-cloud-radiation interactions, and how they are modelled, are one of the largest uncertainties in estimates of climate forcing (Boucher et al., 2013; Forster et al., 2023; Watson-Parris and Smith, 2022). A significant contribution to the uncertainty in indirect aerosol-radiative forcing is due to aerosol from natural sources (Carslaw et al., 2013; Regayre et al., 2020). In the Southern Hemisphere, the Southern Ocean has been a key place of interest to study these uncertainties (eg. see McFarquhar et al., 2021; Schmale et al., 2019), in part due to its remote and relatively untouched environment (Mallet et al., 2023), and in part due to significant radiative biases and uncertainty in climate sensitivity that exist in climate and weather models for the region (Bodas-Salcedo et al., 2014; Protat et al., 2017; Schuddeboom and McDonald, 2021; Regayre et al., 2020; Zelinka et al., 2020). The radiative biases have been attributed to a poor representation of clouds in models. In particular, most models incorrectly simulate ice nucleating particle (INP) processes, which results in models overpredicting ice cloud, and underpredicting super-cooled liquid water clouds (Vergara-Temprado et al., 2018; Vignon et al., 2021).

Poor model representation of emission, aerosol mass, size distribution and composition of sea spray aerosol (SSA) contribute to the uncertainty in natural aerosol (De Leeuw et al., 2011). Both Revell et al. (2021) and Paulot et al. (2020) have demonstrated the influence of SSA on the Earth's climate including on the equilibrium climate sensitivity. However, there is much conflicting literature surrounding the parameterisation of SSA, especially over southern high latitudes, making it difficult to truly trust current results in large-scale modelling. For example, Hartery et al. (2020), Venugopal et al. (2024) and Jaeglé et al. (2011) found that the Gong (2003) SSA flux parameterization over-predicted summertime emissions of SSA, and suggested a reduction of the flux for Southern Ocean conditions. In implementing the Hartery et al. (2020) revised parameterisation into a global climate model Revell et al. (2019) found that reducing the sea spray emissions following Hartery et al. (2020) improved wintertime aerosol optical depth, but adverse effects were found for the summertime. On the other hand, using perturbed parameter ensembles and Southern Ocean aerosol observations, Regayre et al. (2020) found that the SSA flux needed to be scaled up by a factor of 3 (or between 1.6-5.1) to reflect the observed aerosol concentrations. This finding opposes the



50 aforementioned studies showing the SSA is overestimated in models, but is a simple way to increase overall aerosol burden. However, a simple scaling can lack the nuance of more physically driven model changes, especially over regions and seasons.

SSA flux characterisations rely on wind speed with some studies also taking into account the sea surface temperature (SST) (Grythe et al., 2014). In most SSA parameterisations that consider SSTs, the SSA flux increases with increased SSTs, resulting in lower SSA fluxes at high latitudes for equivalent wind speeds. However, the majority of the studies that have deduced these  
55 relationships have had very little high latitude data to form comprehensive statistical relationships (eg. Jaeglé et al., 2011, uses just one voyage in the high latitudes of the Southern Ocean). More recently Sellegri et al. (2023) has suggested that the assumption of the positive SST/SSA relationship may not hold true for the high latitudes of the Southern Ocean, and that this relationship may be modulated by biological activity.

While the uncertainties of SSA fluxes are large when considering the contribution to sea salt aerosol, a further uncertainty is  
60 the contribution of PMO mass from biological activity in the ocean (McCluskey et al., 2017, 2018), which is often modelled as a fraction of the total SSA flux. This flux is often not included in aerosol schemes. As well as contributing to the overall aerosol mass and number, PMO play an important role as a source of ice nucleating particles (INP) (McCluskey et al., 2017), which again, are often not accounted for (Burrows et al., 2022).

Global surface water concentrations and emission of DMS are considered the second largest source of uncertainty with  
65 respect to natural aerosol emissions (Carslaw et al., 2013). In many climate models, DMS is represented by a fixed monthly climatology, based on spatially and temporally biased observations resulting in the climate effects of DMS being poorly understood and poorly captured by climate models (Quinn and Bates, 2011; Fiddes et al., 2018; Bhatti et al., 2023). While a new fixed climatology has been released (Hulswar et al., 2022), online DMS produced by ocean biogeochemical models is desirable to represent variability in the DMS emissions (Bock et al., 2021). Other climatologies developed from satellite records or ma-  
70 chine learning also offer potential alternatives to the observational derived climatologies (Wang et al., 2020; Galí et al., 2018) including to provide time-varying data sets as done in Zhou et al. (2024). Uncertainty around the flux parameterisation also remains, though much literature is now recommending linear parameterisations (e.g. Liss and Merlivat, 1986), which provides a lower emission compared to other methods (Vlahos and Monahan, 2009; Bell et al., 2017; Bhatti et al., 2023).

Not only are the source emissions of aerosol and their precursors poorly captured in climate models, but the subsequent  
75 atmospheric processes they are involved in also contain significant uncertainty. New particle formation (NPF) is frequently observed in the free troposphere (Curtius, 2006; McCoy et al., 2021), though is more rarely detected in the marine boundary layer (BL) (Modini et al., 2009; Brean et al., 2021; Schmale et al., 2019). In a modelling study, Merikanto et al. (2009) estimated 45% of CCN at a 0.2% supersaturation were secondary aerosol formed through nucleation. Within the marine BL, nucleation accounts for 55% of CCN (0.2%) of which 45% were transported from the free troposphere to the marine BL and  
80 10% are formed in the marine BL (Merikanto et al., 2009). Nucleation processes include binary nucleation between sulfuric acid and water (Kulmala et al., 1998), ternary nucleation between sulfuric acid, water and ammonia (Korhonen et al., 1999) and ion-induced nucleation between highly oxidised biogenic vapours (Kirkby et al., 2016). However, parameterisations of NPF are often limited to only binary nucleation. Other biogenic vapours aside from DMS have also been found to nucleate and

are suggested as an important source of CCN in the pre-industrial period (Gordon et al., 2016), however are once again often  
85 neglected in models.

Representative aerosol observations are essential for evaluating and constraining aerosol simulations produced by climate  
models (Regayre et al., 2020; Mallet et al., 2023). However, appropriate, large, datasets are few in the Southern Hemisphere  
in comparison to the Northern Hemisphere, which has added to the difficulty of modelling this region. Recent field campaigns  
have focused on collecting measurements of aerosol, cloud, precipitation and radiation properties, including vessel and land-  
90 based campaigns around Australia and the Southern Ocean (McFarquhar et al., 2021; Schmale et al., 2019), and measurements  
collected from long term monitoring stations (Gras and Keywood, 2017; Hara, 2023). Importantly, these campaigns have  
identified seasonal and latitudinal trends in aerosol, as well as detecting distinct continental (both Antarctic and Australian)  
and free-tropospheric influence on marine air masses (Humphries et al., 2021a; Alroe et al., 2020; Simmons et al., 2021; Gras  
and Keywood, 2017; McFarquhar et al., 2021; Schmale et al., 2019). While there have been a number of modelling studies  
95 that have focused on one or two campaigns in detail (eg. Regayre et al., 2020; McCluskey et al., 2023; Revell et al., 2019)  
there has been no model evaluation of aerosol concentrations for the Southern Ocean/Antarctic that considers a latitudinal and  
seasonal perspective such as that now being discussed in the observational literature. Furthermore, as aerosol parameterisations  
and understanding advances, effort needs to be made to consider these changes together rather than individually. The recent  
suite of campaign data presented by Humphries et al. (2023) provides the perfect opportunity for such an analysis.

100 In this work, we evaluate the performance of the Australian Community Climate and Earth System Simulator - atmo-  
sphere model (ACCESS-AM2), which includes the Global Model of Aerosol Processes (GLOMAP)-mode (GLOMAP) aerosol  
scheme, in simulating CCN and condensation nuclei (particles with a dry diameter greater than 10 nm - N10) using vessel and  
station-based observations in the Australian Antarctic region and Southern Ocean. We further perform a series of experiments  
where we change the aerosol formation from SSA, PMO, DMS and BL NPF to evaluate how these may affect Southern Ocean  
105 and Antarctic aerosol populations. By performing these evaluations, the model biases associated with aerosol-cloud-radiation  
interactions around the Southern Ocean and Antarctic can be better understood and the degree of uncertainty reduced.

### 3 Data and Methods

#### 3.1 ACCESS-AM2

The ACCESS-coupled model (ACCESS-CM2) is the latest Australian coupled climate model which can be run in an atmosphere-  
110 only mode (ACCESS-AM2) (Bi et al., 2020). The ACCESS-AM2 model is configured for the Coupled Model Inter-comparison  
Project phase 6 CMIP6 (Eyring et al., 2016) Atmospheric Model Inter-comparison Project (AMIP). A notable addition to  
the newest versions of ACCESS-CM2 and ACCESS-AM2 is the modal aerosol module Global Model of Aerosol Processes  
(GLOMAP-mode) (Mann et al., 2010), which we will describe shortly.

A detailed description of the ACCESS-CM2 model is provided in Bi et al. (2020), while a description of the atmosphere-  
115 only version of the model is provided in Bodman et al. (2020). Further description of the specific simulation set-up used in this  
work can be found in (Fiddes et al., 2022). To summarise; ACCESS-AM2 uses the UK Met Office's Unified Model Global



Atmosphere (UM10.6 GA7.1) as the atmospheric module, the Community Atmosphere Biosphere Land Exchange model version 2.5 (CABLE2.5) as the land-surface module while aerosol and related processes are simulated by GLOMAP-mode (Bi et al., 2020). ACCESS-AM2 is configured with a horizontal resolution of  $1.25^\circ$  latitude and  $1.875^\circ$  longitude. ACCESS-AM2 has 85 vertical levels, with 50 levels below 15 km and 35 levels above reaching a top height of 85 km. The model has been run for the years 2014-2019 (with 2014 discarded as a spin up year), with daily means as the output.

The ACCESS-AM2 model used has been configured for the CMIP6 AMIP experiment which uses CMIP6 forcings for monthly sea surface temperature (SST), sea ice concentrations (SIC), solar forcing, greenhouse gases (GHGs), volcanic aerosol optical depth, aerosol chemistry and ozone (Eyring et al., 2016). The shared socioeconomic pathway (SSP2-4.5), a middle of the road scenario using emissions described in Feng et al. (2020), was used post-2014 (Fricko et al., 2017; Gidden et al., 2019). The simulations used here have been nudged to the European Centre for Medium-Range Weather Forecasts Reanalysis 5th Generation (ERA5) data outlined in Hersbach et al. (2020) for horizontal wind speed and temperature in the free troposphere at three hourly intervals.

The Community Emissions Data System (CEDS) provided historical (pre-2014) data for anthropogenic emissions of chemically reactive gases, carbonaceous aerosol and  $\text{CO}_2$  (Horsley et al., 2018). Historical global emissions from biomass burning were provided by the Global Fire Emissions Database version 4 with small fires (GFED4s) (Van Marle et al., 2017).

### 3.1.1 GLOMAP-mode

GLOMAP-mode is a comprehensive, two moment, pseudo-modal aerosol scheme. A detailed description of the GLOMAP-mode module is provided in Mann et al. (2010), and Mann et al. (2012). GLOMAP-mode includes sulfate, sea salt, black carbon and organic matter, distributed across five internally mixed modes: soluble nucleation, Aitken, accumulation and coarse modes, and the insoluble Aitken mode (Mann et al., 2010). GLOMAP-mode simulates aerosol in a size-resolved manner and includes primary emission and secondary formation, growth by condensation and coagulation, cloud processing and removal by dry deposition and scavenging (Mann et al., 2010).

For this work, the DMS emission flux from the ocean to the atmosphere is calculated using the surface water DMS climatology outlined in Kettle et al. (1999). The oldest DMS climatology was used in error in the released version of the model (Bi et al., 2020), however the majority of experiments in this study will be evaluated using the Lana et al. (2011) climatology inline with the GA7.1 configuration (Walters et al., 2019). The DMS flux equation used is provided by Liss and Merlivat (1986). Further description and discussion about the uncertainties of DMS climatologies and flux parameters can be found in Fiddes et al. (2018) and more recently in Bhatti et al. (2023). We note that the DMS emission is scaled by a factor of 1.7 to take into account the lack of PMO, which are not switched on by default (Mulcahy et al., 2018). SSA emission fluxes are calculated using the wind-speed parameterization source function developed by Gong (2003). NPF by the binary homogeneous nucleation of water and sulfuric acid in the free troposphere is parameterised according to Kulmala et al. (1998), while BL NPF is not switched on. Dust emissions are determined externally to GLOMAP-mode using a binning method outlined in Woodward (2001). Other trace gas and primary aerosol emissions from anthropogenic and terrestrial sources include volcanic sourced and industrial  $\text{SO}_2$ , biomass burning and monoterpenes. These are prescribed according to CMIP6 protocols (Eyring et al., 2016).



| Simulation | Aerosol configuration  | Reference   |
|------------|--|---|
| Control*   | As described in Section 3.1.1 using the Kettle et al. (1999) DMS climatology | Mann et al. (2010); Kettle et al. (1999)                        |
| Control    | As for Control* but with the Lana et al. (2011) DMS climatology              | Mann et al. (2010); Lana et al. (2011)                          |
| BL NPF     | Boundary layer nucleation turned on  | Metzger et al. (2010)   |
| SSA gust   | Use max wind gust instead of mean wind in the SSA flux                       | NA  |
| PMO        | Primary marine organics aerosol emission turned on                           | Gantt et al. (2012)   |
| H22 DMS    | Revision 3 DMS climatology used  | Hulswar et al. (2022)   |
| OM2 DMS    | Daily DMS derived from ACCESS-Ocean Model (OM) 2                             | Bock et al. (2021); Kiss et al. (2020); Hayashida et al. (2021) |
| PMO + H22  | Combined H22 DMS climatology scaled to 1.0 with PMO switched on              | Hulswar et al. (2022); Gantt et al. (2011)                      |

**Table 1.** The eight simulations run to evaluate aerosol concentrations in the Southern Ocean. Each experimental simulation describes a change to the way aerosol are produced but are otherwise the same as the Control (not the Control\*)

## 3.2 Experiment simulations

For this study, eight model runs were analysed for cases with varying changes to aerosol formation or sources. The control simulation is setup as per the description in the previous section, while each experiment varies from this set-up, which is summarised in Table 1.

### 155 3.2.1 BL NPF

In our first experimental simulation, which we refer to as the ‘BL NPF’ simulation, we use the Metzger et al. (2010) BL NPF parameterisation, which involves the organic-mediated nucleation of  $H_2SO_4$  and an organic compound (*NucOrg*). The nucleation rate equation outlined in Metzger et al. (2010) is shown by Equation 1, where  $J_{1.5}$  is the nucleation rate of 1.5 nm dry diameter stable particles,  $k$  is the rate constant, and  $m$  and  $n$  are the reaction orders for sulfuric acid and the organic compound respectively. In ACCESS-AM2 the organic compound is provided by secondary organic carbon precursors (assumed to be  
160 monoterpenes, noting that GLOMAP-mode does not include isoprene).

$$J_{1.5} = k[H_2SO_4]^m[NucOrg]^n \quad (1)$$

### 3.2.2 SSA emissions

In this experiment, ‘SSA gust’, we increase the SSA flux to better match observed total aerosol concentrations (not SSA aerosol  
165 alone), as suggested by Regayre et al. (2020). However, instead of a simple scaling by a factor of 3 as suggested by Regayre et al. (2020), we have instead substituted the daily mean horizontal wind speed with the daily mean horizontal maximum wind gust at 10m ( $u_{mx10}$ ). This reflects the higher wind speeds observed in the Southern Ocean compared to elsewhere, and the fact that over the course of an hour (the model time steps that SSA is calculated), much of the SSA is likely to come from these



gusty periods. GLOMAP-mode uses the Gong (2003) parameterisation (Equation 2) where the size binned flux emission of sea  
 170 spray  $\frac{dF}{dr}$  depends on the particle radius at 80% humidity ( $r$ ), the horizontal wind at 10 m ( $u_{10}$ ), and a shape parameter of the  
 size distribution  $\Theta$ ).

$$\frac{dF}{dr} = 1.373u_{m.x10}^{3.41}r^{-A}(1 + 0.057r^{3.45}) \times 10^{1.607e^{-B^2}} \quad (2)$$

$$A = 4.7(1 + \Theta r)^{-0.017r^{-1.44}} \quad (3)$$

$$B = \frac{(0.433 - \log(r))}{0.433} \quad (4)$$

### 175 3.2.3 PMO

The experiment ‘PMO’ switches on PMO aerosol formation, via the SSA function, which currently assumes all aerosol to be  
 salt. This empirical parameterisation uses the 10 m wind speed ( $u_{10}$  in  $\text{m s}^{-1}$ ), ocean chlorophyll-a ( $CHL$  in  $\text{mg m}^{-3}$ ) and sea  
 spray particle dry diameter ( $D_p$  in  $\mu\text{m}$ ) to calculate the organic mass fraction ( $frac_{OM}$ ) of the SSA (Equation 5). We note  
 that the wind speed function is used here to represent surface tension of the sea surface microlayer (surface accumulation of  
 180 organics). Higher wind speeds break this layer up, resulting in fewer organics being lofted into the atmosphere. To calculate the  
 mass flux of organics ( $flux_{OM}$  in  $\text{g m}^{-2} \text{s}^{-1}$ ) the fraction of organic material is applied to the volume flux of sea salt aerosol  
 ( $V_{SSA}$  in  $\text{cm}^3 \text{m}^{-2} \text{s}^{-1}$ ) multiplied by the density of sea spray aerosol particle ( $\rho_{SSA}$  in  $\text{g cm}^{-3}$ )(Equation 6). The organic  
 mass flux is then added to the Aitken mode, 25% to the soluble mode, and 75% to the insoluble mode.

$$frac_{OM} = \frac{1}{1 + 0.03 \exp(6.81D_p)} + \frac{0.03}{1 + \exp(3(-2.63CHL) + 3(0.18(u_{10})))} \quad (5)$$

$$185 flux_{OM} = frac_{OM} \times V_{SSA} \times \rho_{SSA} \quad (6)$$

We note that the default DMS emissions remain at the 1.7 scaling in this simulation. We have tested reducing the the DMS  
 emissions scaling to 1.0 with the PMO switched on in a further simulation in combination with the new DMS climatology  
 described below. We have also tested this parameterisation with the increased SSA experiment described previously, where the  
 wind gust is used for the SSA flux rather than the mean wind. For this experiment, we have not used the wind gust in the PMO  
 190 calculations, as they are representative of the depth of the microlayer, not the actual flux of matter.

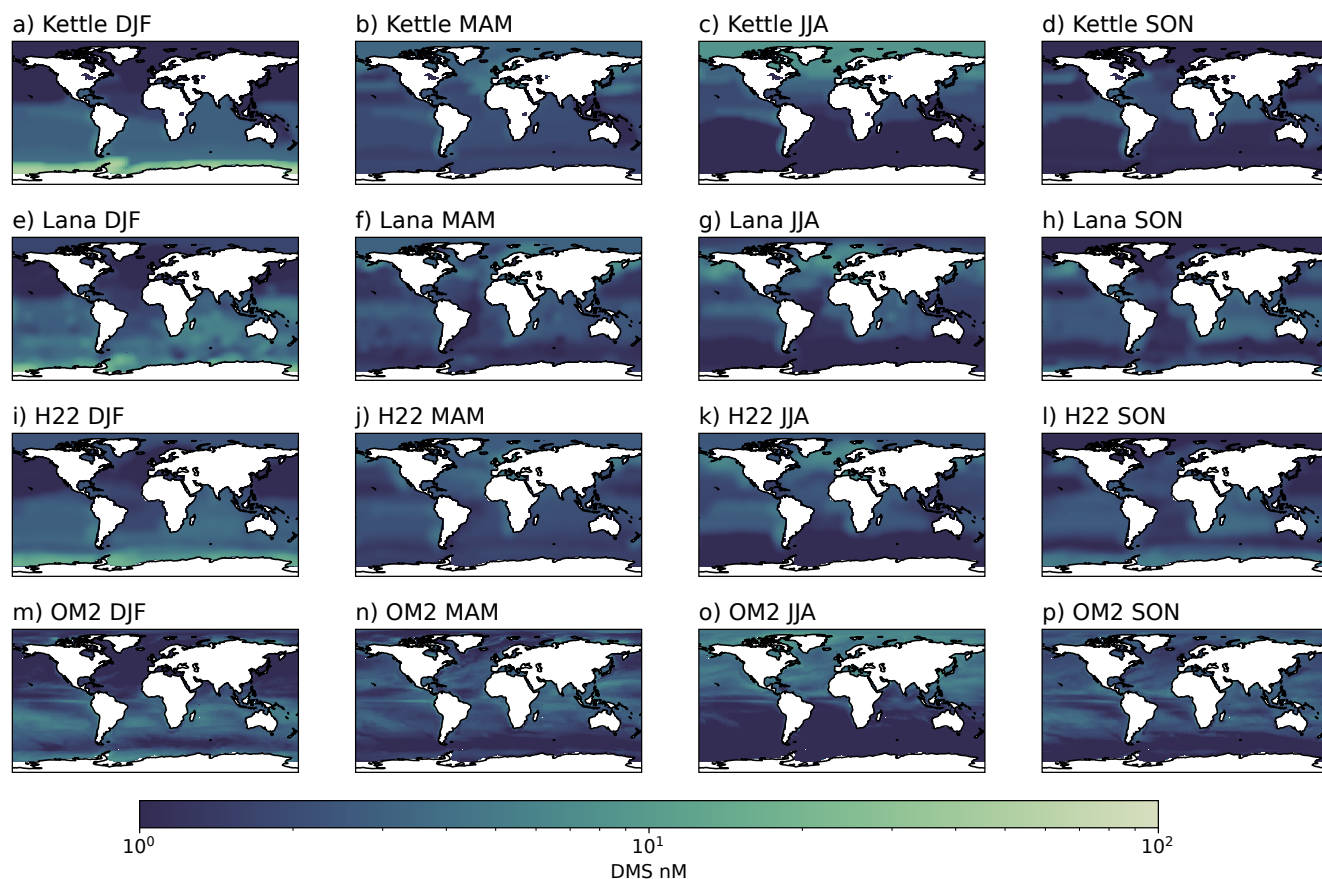


**Figure 1.** The seasonal mean DMS (nM) climatologies (from left to right DJF, MAM, JJA, SON) for, from top to bottom: Kettle et al. (1999), Lana et al. (2011), Hulswar et al. (2022) and the daily resolving OM2 parameterisation.

### 3.2.4 DMS climatologies

The Control\* simulation uses the original Kettle et al. (1999) DMS climatology, which is used by default in the ACCESS model despite the recommendation of using the Lana et al. (2011) climatology, as described in Section 3.1.1. All DMS climatologies are shown by their seasonal means in Figure 1.

195 The ‘H22’ experiment refers to the use of the most recent DMS climatology produced by Hulswar et al. (2022). This climatology uses significantly updated observations and methodology to account for observational biases, seasonality of biogenic regions and the interpolation of missing data.

We have also produced an offline interannual daily DMS dataset derived from output of the ocean component of ACCESS, ACCESS-OM2, referred to as ‘OM2 DMS’. Details of ACCESS-OM2 and the interannual simulation used to produce the  
200 DMS output can be found in Kiss et al. (2020) and Sections 2.1 and 3.1 of Hayashida et al. (2021). ACCESS-OM2, in this





case not coupled to AM2, was driven by the ACCESS-AM2 atmospheric boundary conditions from the Control\* experiment, which are usually provided by reanalysis.

The parameterisation used here to estimate the DMS surface water concentration has been developed for the North Pacific ocean (Aranami and Tsunogai, 2004). Little testing for such parameterisations have been done to this point for the Southern Ocean, in part due to very limited observations. However, this is seen as a starting point for developing online DMS in the ACCESS-OM2 model. Furthermore, as Bhatti et al. (2023) notes, time-varying datasets are seen as preferable over the fixed monthly climatologies given their ability to represent day-to-day fluctuations of the DMS production. The OM2 parameterisation considers two regimes based on the ratio of chlorophyll-a concentration ( $CHL$  in  $\text{mg m}^{-3}$ ) to the ocean mixed layer depth ( $MLD$  in m), as shown in Equation 7 below from Bock et al. (2021). Chlorophyll-a concentrations are calculated offline in ACCESS-OM2 assuming a fixed nitrogen-to-chlorophyll ratio following Oke et al. (2013). Under a low ratio, DMS concentrations depend only on the  $MLD$ , where DMS concentrations are considered to be more diluted with greater  $MLDs$ . Only under a high ratio, where either high  $CHL$  or moderate-low  $CHL$  and a shallow  $MLD$ , did the authors find that DMS was correlated with  $CHL$ , hence necessitating the two conditional equations.

$$DMS = \begin{cases} \frac{60}{MLD} & \text{if: } \frac{C}{MLD} < 0.02 \\ 55.8 \cdot \frac{CHL}{MLD} + 0.6 & \text{if: } \frac{CHL}{MLD} \geq 0.02 \end{cases} \quad (7)$$

### 215 3.3 Field Observations

The ACCESS-AM2 model aerosol scheme was evaluated against a number of observations from field campaigns carried out on research vessels and at land-based research stations. A map showing the tracks for vessel-based campaigns and locations of research stations is shown in Figure 2. Measurements of N10 number concentrations, and CCN concentrations at 0.5% supersaturation were used as these variables were available for most observation sources. Brief summaries for each of the field campaigns and their respective instruments and operations are provided below.

#### 3.3.1 RVI

The Research Vessel Investigator (RVI) is a marine research vessel which has included 'underway' N10 and CCN measurements since 2015. The RVI is also the world's first World Meteorological Organisation Global Atmosphere Watch (WMO GAW) mobile station capable of undertaking continuous atmospheric composition measurements. Aerosol number concentrations are measured using a modified condensation particle counter (TSI CPC model 3772, Shoreview, Minnesota, United States) while CCN number concentrations are measured using a CCN counter (CCNC, Model CCN-100, Droplet Measurement Technologies, Longmont, Colorado, United States). The CPC on the Investigator operates at a frequency of 1 Hz which was used to calculate daily medians for the analysis. The CCNC sampled 1 Hz CCN at 1.0, 0.6, 0.5, 0.4, 0.3 and 0.2% supersaturations sequentially, resulting in 10 minutes at each setting and the sequence repeated hourly. The atmospheric instruments on the RVI can be affected by exhaust emissions from the ship's engine combustion and waste incineration. The RVI aerosol data

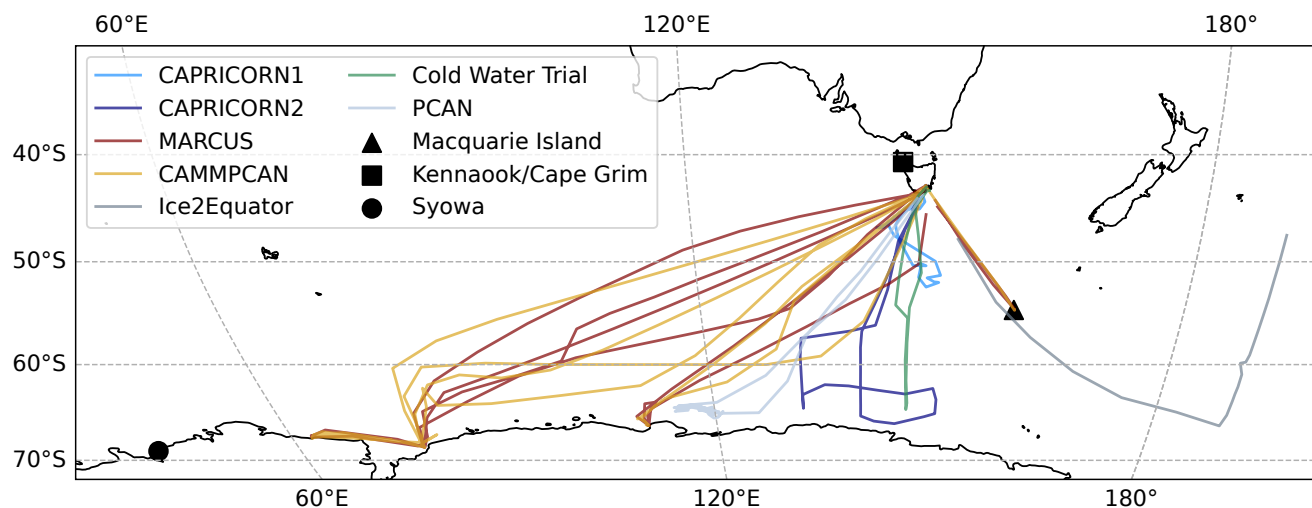


**Figure 2.** Overview of the field observations used in this work. Blues (CAPRICORN 1 and 2), green (Cold Water Trial) and greys (Ice2Equator and PCAN) shows measurements from campaigns aboard the RV Investigator, red illustrates the MARCUS campaign while yellow shows the CAMMPCAN campaign, both aboard the RSV Aurora Australis. The ship voyage tracks are the daily mean ship location. In black are the locations of the land-based stations of Kennaook/Cape Grim (square), on Tasmania's north-west coast, and Macquarie Island in the middle of the Southern Ocean (triangle) and Syowa (circle) on the Antarctic coast.

therefore must be exhaust filtered using the algorithm described in Humphries et al. (2019), and manually reviewed in order to identify and remove periods when ship exhaust had been sampled.

The observations used in this study have been made during specific atmospheric focused voyages, after which stringent quality control has been undertaken. These voyages include the Cold Water Trials over January-February 2015; Polar Cell  
235 Aerosol Nucleation (PCAN) over January-March 2017; Ice2Equator over April-June 2016; and Clouds, Aerosols, Precipitation, Radiation, and atmospheric Composition Over the southern ocean (CAPRICORN) 1 and CAPRICORN 2 which occurred over March-April 2016 and January-February 2018, respectively. These voyages are described in more detail in Humphries et al. (2023). We note that CCN data is available for all voyages, but N10 data was not available for PCAN, CAPRICORN1 and Ice2Equator. We have limited Ice2Equator data to south of 47.5°S to avoid terrestrial influence from New Zealand.

### 240 3.3.2 MARCUS

During the period of October 2017 to March 2018, the Research Survey Vessel Aurora Australis (AA) hosted the Measurements of Aerosol, Radiation and Clouds over the Southern Ocean (MARCUS) campaign. The MARCUS campaign utilised the Atmospheric Radiation Measurement (ARM) project Mobile Facility including the Aerosol Observing System (Uin et al.,  
245 completed resupply voyages between Hobart and the Mawson, Davis, Casey and Macquarie Island stations (McFarquhar et al.,



2021). During MARCUS, the Aerosol Observing System collected measurements of aerosol number concentrations using a CPC (TSI CPC model 3772, Shoreview, Minnesota, United States) sampling at a frequency of 1 Hz (Humphries et al., 2021a). A CCN counter (CCNC, Model CCN-100, Droplet Measurement Technologies, Longmont, Colorado, United States) was used to determine CCN concentrations at supersaturations of 0.0, 0.1, 0.2, 0.5, 0.8 and 1.0% for 10 minutes each over an hour  
250 (Humphries et al., 2021a). Due to the setup of the ARM equipment near the AA exhaust pipe, a majority of the observations were exhaust contaminated and required filtering (Humphries et al., 2021a). The data were exhaust filtered using an exhaust identification algorithm outlined in Humphries et al. (2019), and then manually using air composition data (Humphries et al., 2021a).

### 3.3.3 CAMMPCAN

255 In the following summer the AA completed the same re-supply voyages from October 2018 to March 2019 with the Chemical and Mesoscale Mechanisms of Polar Cell Aerosol Nucleation (CAMMPCAN) campaign onboard, including the Atmospheric Integrated Research facility for Boundaries and Oxidative eXperiments (AIRBOX) mobile facility. The CAMMPCAN campaign hosted a CPC (TSI CPC model 3772, Shoreview, Minnesota, United States) sampling at a frequency of 1 Hz, and a CCNC, Model CCN-100, Droplet Measurement Technologies, Longmont, Colorado, United States) to measure CCN concentrations at supersaturations of 0.0, 0.1, 0.2, 0.5, 0.8 and 1.0% for 10 minutes each over an hour. Black carbon measurements at  
260 5 minute averages were used to initially filter the data for ship exhaust influence, with a threshold value of  $70 \text{ ng}/\text{m}^{-3}$  used. Following this, the same exhaust filtering as described in Humphries et al. (2019) were applied to these data. Manual inspection and filtering of the resultant data was then completed using concurrent CO and CO<sub>2</sub> measurements.

### 3.3.4 kennaook / Cape Grim

265 kennaook / Cape Grim (KCG) is an atmospheric monitoring station located in the northwest of Tasmania (40°41'S, 144°41'E) that has been operating since the mid 1970s (Gras and Keywood, 2017). The KCG station is positioned on a cliff 94 m above the sea level to maximise observations from the Southern Ocean which represents primarily pristine marine air that are mostly unaffected by anthropogenic influences (Gras and Keywood, 2017). Atmospheric particle sampling procedures at KCG generally follow the WMO GAW Aerosol Programme Recommendations (World Meteorological Organization (WMO), 2016).  
270 Measurements of aerosol number concentrations were made using a set of condensation particle counters (TSI 3760/TSI 3010) running at a frequency of 1 Hz and averaged over minutely intervals (Gras and Keywood, 2017). CCN concentrations primarily at 0.5% supersaturation were measured using a CCN counter (CCNC, Model CCN-100, Droplet Measurement Technologies, Longmont, Colorado, United States) (Gras and Keywood, 2017). N<sub>10</sub> measurements were available for the period 2016-2018 while CCN data was available for 2015-2018. Further station descriptions for KCG are provided in Gras and Keywood (2017).  
275 The data presented here is the baseline filtered data (as described in Gras and Keywood, 2017), identifying only air that has come from the Southern Ocean where the wind direction was between 190 and 280° and the radon concentration is below 100 mBq.



### 3.3.5 Macquarie Island

Macquarie Island (MI) is located at 54.5°S, 158.9°E and is the site of a year-round research station. The position of MI in  
280 the Southern Ocean makes it a suitable location for monitoring cloud, radiation precipitation and aerosol properties over the  
region. The MI research station hosted the Macquarie Island Cloud and Radiation Experiment (MICRE) which ran from March  
2016 to March 2018. Measurements of N10 were made using a modified condensation particle counter (TSI CPC model 3772,  
Shoreview, Minnesota, United States) at a frequency of 1 Hz which were averaged to hour intervals. A CCN counter (CCNC,  
Model CCN-100, Droplet Measurement Technologies, Longmont, Colorado, United States) was used to determine  
285 CCN concentrations at supersaturations of 0.2, 0.3, 0.4, 0.5, 0.6, 1.0% each hour. The detailed aerosol set-up is described in  
Humphries et al. (2023). A campaign report for MICRE is provided in Marchand (2020) and McFarquhar et al. (2021), which  
includes a summary of the experiment objectives and instruments used.

### 3.3.6 Syowa

Syowa Station is an Antarctic research station located on East Ongul Island in Lutzow-Holm Bay (69.0°S, 39.0°E). The station  
290 is coastal and surrounded by seasonally varying sea-ice year round. A detailed description of SYO and the station operations is  
provided in Hara et al. (2011, 2021). The station operates several CPCs (TSI model 3010, Shoreview MN, USA) that have been  
collecting aerosol measurements since 1997. For this study only aerosol measurements from 2015 were used for evaluation, to  
match with the availability of model output, though the observations include data as far back as 2004. Measurements of N10  
were available as daily means and medians. Measurements of CCN were not available. The SYO data was included to provide  
295 a long term, high latitude record of aerosol number concentrations that could be contrasted with northern and mid-latitude  
stations of KCG and MI. The data for SYO is publicly accessible in Hara (2023).

## 3.4 Analysis methods

Analysis methods used to evaluate model performance are described below, including details of how the evaluation has been  
carried out and how air masses/regions have been divided for analysis. Some evaluation of the models meteorology has been  
300 carried out, but is not shown in this work. It was found to be satisfactory, which is in line with our expectations due to nudging.

### 3.4.1 Aerosol evaluation

N10 has also been chosen for analysis over other size cutoffs given its availability across voyages/stations. The CCN measured  
at a supersaturation of 0.5% is the most commonly measured saturation across all campaigns used in this study, allowing  
for consistent comparison. However, the model does not provide CCN at a specific supersaturation, but provides the size  
305 distribution from which we can calculate CCN activation dry diameters. To identify an equivalent activation diameter for  
the 0.5% supersaturation, we have used the method described in Petters and Kreidenweis (2007) Equation 10 and Table 1  
to identify a suitable hygroscopicity parameter ( $\kappa$ ) from which we can calculate the critical activation diameter. We have  
assumed that the majority of model aerosol is internally mixed  $\text{H}_2\text{SO}_4$ , i.e most aerosol have a coating of  $\text{H}_2\text{SO}_4$  and therefore,



310  $\kappa = 0.9$ . This results in a dry diameter of approximately 40 nm. The mean daily CCN40 particle concentration (aerosol particles with a dry diameter greater than 40 nm) was then calculated from the model size distributions. Our method is inline with assumptions made in previous GLOMAP-mode studies (e.g. Mann et al., 2010). However, we note that we also tested the activation ratios with an externally mixed assumption for the modelled aerosol, which gave an activation diameter of 35 nm, which we believe to be unrealistic for this region (Fossum et al., 2018). The full workflow for these tests can be found in the linked GitHub repository for this work.

315 Aerosol evaluation was performed only on the days in which observational data was available, ensuring a like-for-like comparison. At KCG, we have used the exact model gridbox that the station is located in, as choosing a gridbox to the southwest of the station resulted in poorer performance. This could be due to the fact that moving even one gridbox away diagonally, in a very coarse resolution model, is enough to change the synoptic circulation compared to that experienced at the station. We also recognise that we have not performed a similar baseline filtering to the model (in part due to lack of radon in the model),  
320 but have applied the same baseline filtering to the model as what was developed for the observations. This may introduce some bias given the coarse resolution of the model, however, our initial analysis of the meteorology indicates that the large-scale flow in the model is comparable to the observations.

### 3.4.2 Statistical Methods

Model data was extracted by linearly interpolating model grid coordinates using the inbuilt python Xarray function (Hoyer and  
325 Hamman, 2017) to the mean daily latitude and longitude locations of the observations.

The data was grouped by latitudinal sectors defined in Humphries et al. (2023). The sectors are defined as a northern region ( $<45^{\circ}\text{S}$ ), the mid-latitudes ( $45\text{--}60^{\circ}\text{S}$ ), a sub-polar region ( $60\text{--}65^{\circ}\text{S}$ ) and the Polar Cell ( $>65^{\circ}\text{S}$ ).

### 3.4.3 Radiation evaluation

We have used the top of atmosphere outgoing shortwave radiation from the Clouds and the Earth's Radiant Energy System  
330 (CERES) Syn1Deg product (Doelling et al., 2013, 2016). More information on this product and its use for this study can be found in Fiddes et al. (2022). The radiation evaluation was carried out for the full 5 year period, as satellite products are also available over this time.

## 4 ACCESS-AM2 Aerosol evaluation and sensitivity testing

### 4.1 N10

335 To determine how the control run performs against the observations, Figure 3 shows the N10 concentration seasonal cycle for KCG, MI and Syowa. For KCG, the model underestimates the baseline observations by 53% on average, with the largest relative underestimations in winter (60%) and the smallest in autumn (41%). The control run does appear to capture a seasonal cycle (see Figure 3a), however, it is not as pronounced as the observations. The timings of the seasonal minima and maxima

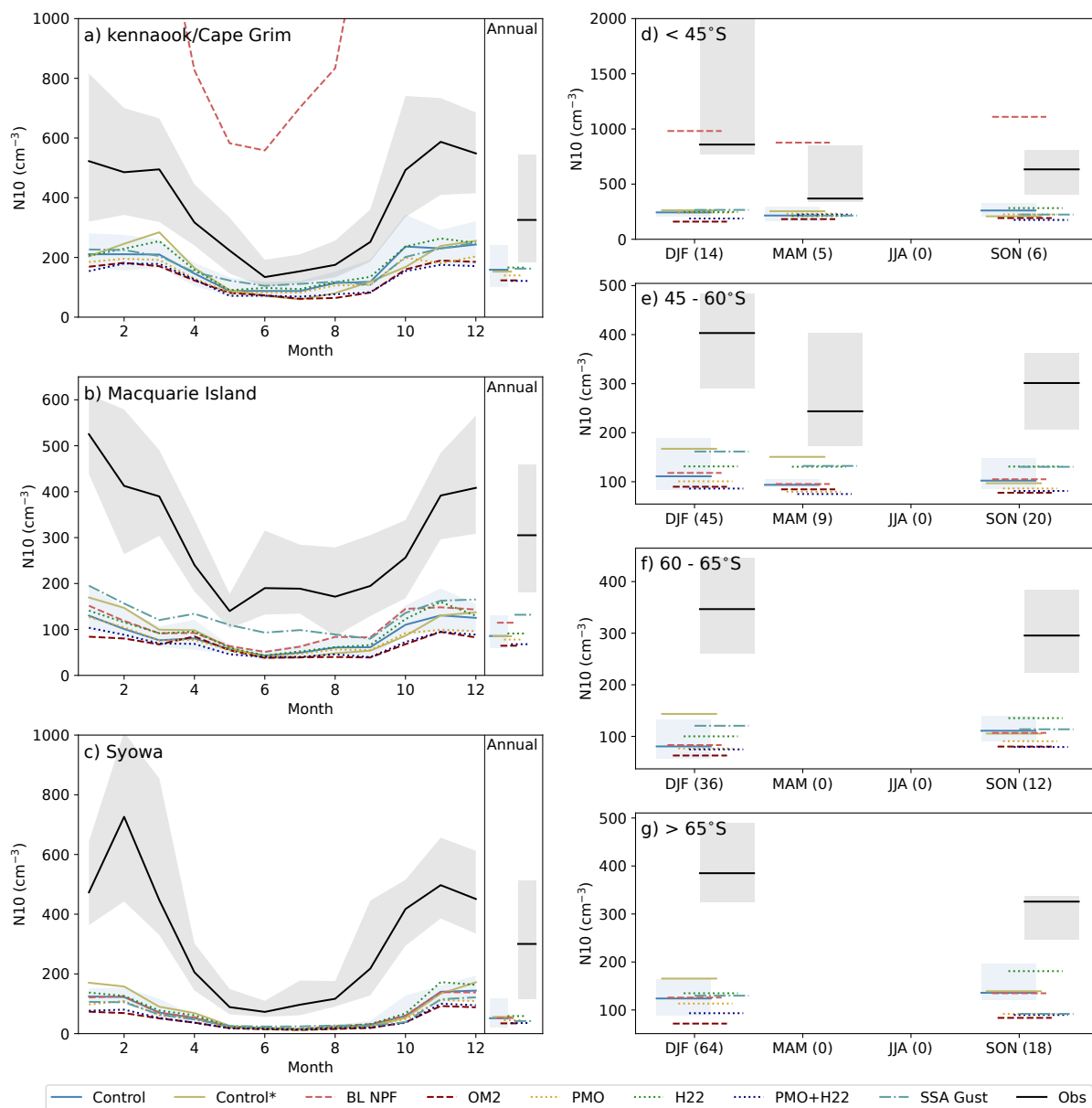


**Figure 3.** The monthly and annual median concentrations of N10 for at (a) kennaook/Cape Grim (KCG), (b) Macquarie Island and (c) Syowa and the seasonal medians for voyage data by latitude (d) north of  $45^\circ\text{S}$ , (e)  $45-60^\circ\text{S}$ , (f)  $60-65^\circ\text{S}$  and (g) south of  $65^\circ\text{S}$ . For all, the 25th and 75th percentiles are shown by the shaded range for the observations and control run. The observations are shown in black, while each of the model simulations are shown in colour including the control (blue), BL NPF (light red), H22 DMS (green), OM2 DMS (dark red), PMO (yellow), PMO + H22 (navy) and SSA Gust (teal). We note that for KCG in (a) the BL NPF simulation shows N10 values that exceed  $1500\text{ cm m}^{-3}$  in the warmer seasons which we believe to be unrealistic, hence we have limited the y-axis for readability. We also note that the number of observations making up the voyage values are shown in the x-axis.



have been correctly simulated. The standard deviation is also underestimated on average, where the control run for KGC has a  
340 mean standard deviation of  $123 \text{ cm}^{-3}$  compared to  $342 \text{ cm}^{-3}$  in the observations.

For MI, the control run underestimates the observations by 69% throughout the timeseries, with summer being the most  
underestimated (71%) and spring the least (64%). The control run also does not capture the seasonal minima at the correct time  
of year, which in the observations is shown in May after a steep decline through autumn, whilst for the model is shown in June  
(Figure 3b). The model's seasonal cycle is very flat compared to the observations, indicating both missing sources of aerosol  
345 and missing seasonal processes, although we note that we only have two seasonal cycles to analyse. The model again shows  
little variance in the winter periods, with larger variance in the summer. On average the standard deviation is observed to be  
 $198 \text{ cm}^{-3}$  for MI and simulated to be  $68 \text{ cm}^{-3}$ .

Finally, Syowa, the station furthest south, shows the largest bias in aerosol concentrations from the model, with an overall  
underestimation of 78%, which is largest in winter and autumn (both 81%), and smallest in summer (74%). Similar to MI,  
350 Syowa has a minimum in May that is not captured by the model, which simulates the minima in August instead. The summer-  
time maxima at Syowa is shown in the observations to occur in February, whilst is simulated in the control in December (Figure  
3c). This may be due in part to the model's treatment of sea ice and its influence on aerosol formation. On average the standard  
deviation of N10 for Syowa simulated to be  $66 \text{ cm}^{-3}$  compared to the observed  $427 \text{ cm}^{-3}$ . The significant underestimation of  
N10 and the flat seasonal cycle at Syowa points to a considerable underestimation of small sized aerosol in the polar region,  
355 likely a missing source, such as new particles formed from biogenic precursors.

Figure 3d-g shows the seasonally and latitudinally grouped N10 medians for all the voyages. The control run (light blue)  
underestimates N10 in all seasons and latitudes. It also has considerably less variability (not shown), although we note the very  
small sample size in some instances (shown in x-axis labels). The largest underestimation occurs in DJF for all regions: 74%,  
72%, 74% and 71% from north to south, though we also note that DJF has the most observations of all seasons.

We now consider the experimental runs. At KCG, switching on BL NPF (light red) has a very strong impact across the year,  
with the N10 concentrations going from an annual underestimation of 53% to an over estimation of 290%. For the voyage  
based observations north of  $45^\circ\text{S}$  (Figure 3d), we can also see a large increase in N10 across all seasons, with the largest  
being in spring, though we note very few observations. For DJF, the BL NPF simulation is now overestimates the observations  
by 33%. For the same season at KCG the simulation over performed by 266%. The difference in these two results may be  
365 explained by the influence of land and the associated volatile organic compounds (VOCs) occurring due to the coarse model  
resolution, however, we note that this overestimation of N10 at KCG was not improved by moving the model gridbox further  
over the ocean, possibly also indicating an issue with the marine biogenics.

For MI, the inclusion of BL NPF increases the N10 concentrations marginally (underestimated by 61% compared to control  
of 69%). MI, a small island in the SO, is influenced by marine biogenic activity, though we note that this is not a very productive  
370 region of the SO according to the Lana et al. (2011) climatology (DMS concentrations are low), explaining the lack of response  
to the BL NPF. We also suggest that a lack of simulated VOCs to help mediate NPF plays a role. Similar marginal results are  
found in the mid-latitude voyage data (Figure 3e).



For Syowa, turning on BL NPF has little impact. This result is unsurprising given the NPF mechanism being employed in the model, which as discussed earlier, is an organically mediated mechanism, relying on prescribed monoterpenes, which are at their largest over terrestrial regions. Recent literature has shown that VOCs, such as isoprene, are important for the pristine marine environments of the Southern Ocean (Ferracci et al., 2024), especially in the marginal ice zones (MIZ) where biogenic activity is high. However these emissions are currently not considered by GLOMAP-mode. Additionally, the biological activity associated with sea ice is not explicitly included in the DMS climatologies, suggesting a potential missing source. This is a key area for development for GLOMAP-mode.

Turning on PMO (yellow), which adds aerosol into the Aitken mode, results in little change to the model performance in terms of N10. A small reduction in aerosol number across all stations and most voyage observations compared to the control run is found, moving further away from the observed N10 values. The addition of PMO aerosol may increase the rate at which aerosol are coagulating and growing, reducing the overall number of smaller sized aerosol, and resulting in fewer overall, but larger sized aerosol. This is found across all regions and seasons.

The original Kettle et al. (1999) DMS climatology in the Control\* simulations shows larger N10 values in the summer months for most regions whilst having minimal impacts at other times. This is especially the case for high latitude regions where the summertime DMS concentrations are very large compared to the more recent climatologies. The OM2 climatology (maroon) reduces the aerosol concentration for all sites and voyage points compared to the control. This suggests that the simple parameterisation used is not suitable for the Southern Ocean despite being a daily, time-varying climatology. We also note that the correlation values between the observations and simulations do not significantly improve between the control and OM2 simulations. The H22 DMS climatology (green) increases N10 concentration for all stations and latitudes largely in the warmer months and shoulder seasons, reflecting a slight improvement compared to the control run.

Increasing the SSA flux (teal) by using the wind gust instead of the mean wind speed again has only marginal results for the N10 concentrations, with the largest increases seen at MI and the mid-latitude voyage band. At MI the annual bias goes from 69% underestimated to 55%, while a decrease in the N10 bias by 4% is found at KCG and no change is found at Syowa. In the high latitude voyage data the SSA flux changes reduce the model's skill in producing N10 aerosol by approximately 17% in SON, with little change in DJF.

Finally, we present a PMO simulation combined with the H22 DMS climatology, with the flux scaled back to 1.0 x (from 1.7 x in the control) in navy. The combination of a scaled back sulfur source and an additional source of Aitken sized aerosol to act as surfaces for condensation has resulted in fewer N10 sized aerosol across all stations (an annual increase in bias of between 5-11%). A similar result is found for all voyage data. This has a number of implications, for example: that the source of biogenic precursor gases may be too low across all regions; that the SSA or PMO sources should include some aerosol at smaller sizes; that nucleation mechanisms are incorrect. A detailed study with a comprehensive suite of size and compositionally resolved observations in combination with the simulated budget terms for the aerosol (eg. mass transfer across modes) is required to disentangle these processes.



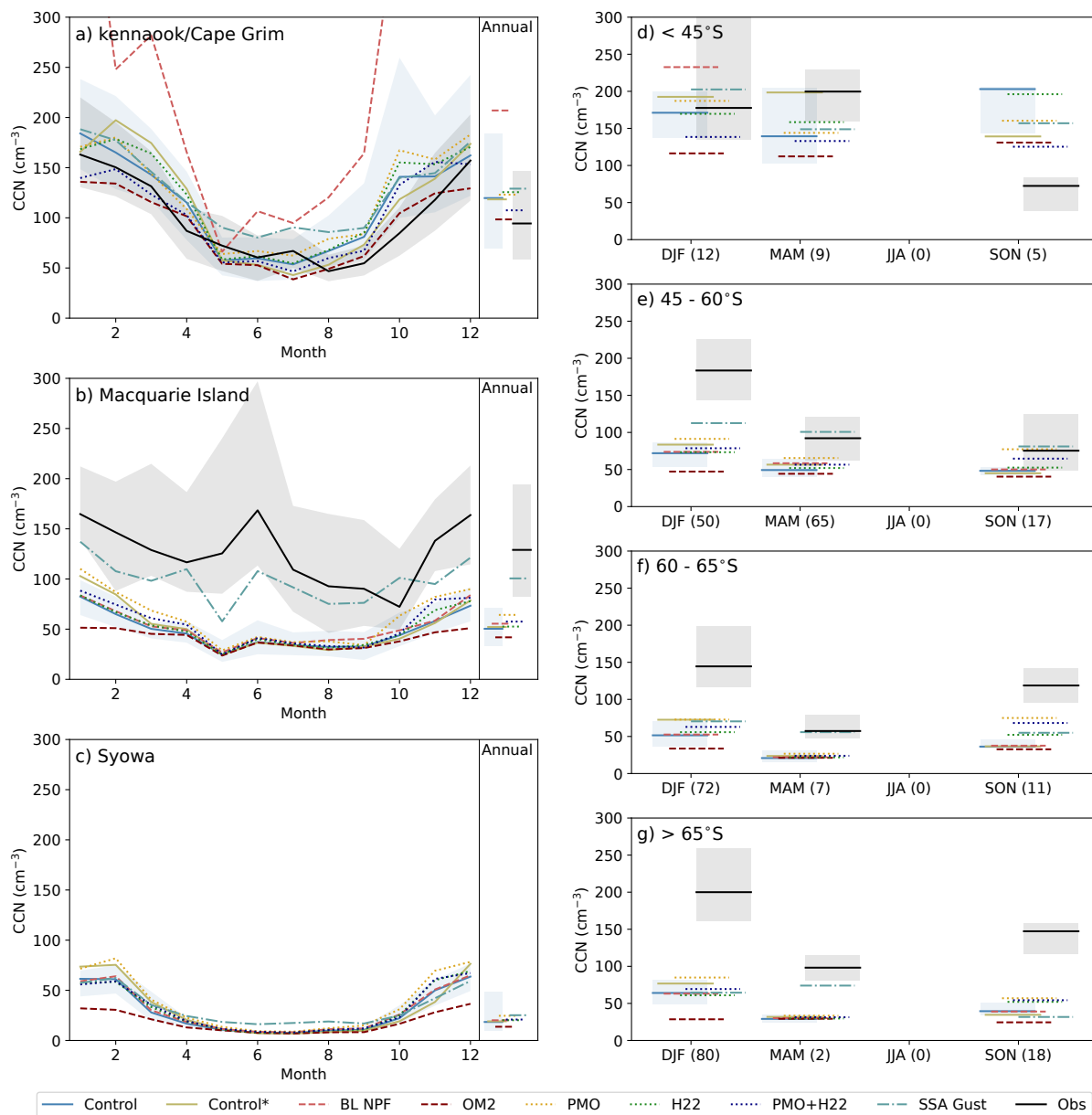


**Figure 4.** The monthly and annual median concentrations of CCN40 for at (a) kennaook/Cape Grim (KCG), (b) Macquarie Island and (c) Syowa and the seasonal medians for voyage data by latitude (d) north of  $45^\circ\text{S}$ , (e)  $45-60^\circ\text{S}$ , (f)  $60-65^\circ\text{S}$  and (g) south of  $65^\circ\text{S}$ . For all, the 25th and 75th percentiles are shown by the shaded range for the observations and control run. The observations are shown in black, while each of the model simulations are shown in colour including the control (blue), BL NPF (light red), H22 DMS (green), OM2 DMS (dark red), PMO (yellow), PMO + H22 (navy) and SSA Gust (teal). We note that there are no observations for Syowa and that the number of observations making up the voyage values are shown in the x-axis



## 4.2 CCN

We now consider the larger sized aerosol range, examining observed CCN at 0.5% supersaturation (following Humphries et al., 2023), which we compare to CCN40 in the model. We recognise that the assumptions made to compare these two fields are imperfect, however, until observed size distributions are available, from which we can apply the same cut-off, our method is  
410 the best achievable.

For baseline KCG observations, as shown in Figure 4a, the control run overestimates the observations by 20%. The control run simulates the monthly minima in July, compared to August in the observations and has flatter wintertime dip in CCN concentrations. It captures the January maxima well. The annual standard deviation is  $99 \text{ cm}^{-3}$  compared to the observed  $69 \text{ cm}^{-3}$ .

415 For MI, we can see that the model performs far worse compared to KCG, with an overall underestimation of 58% and a standard deviation of only  $29 \text{ cm}^{-3}$  compared to  $100 \text{ cm}^{-3}$ . The model correctly simulates the summer time maxima in January, but struggles to get the observed minima correct (October in observations compared to May). In the observations, Humphries et al. (2023) noted a significant wintertime peak in CCN concentrations (Figure 4b). The authors speculated that this could be due to increased sea spray aerosol associated with higher winds during the winter. However, they noted that a large part of the  
420 second winter season was missing so we cannot rule out the possibility of this peak being due to a few outlier events. Given the limited availability of wintertime data we cannot say if the frequency of large, individual events is common or not for this time of year. The control run shows a very small wintertime peak for the same period, but of much smaller magnitude to what was observed, which could indeed be driven by sea spray, long range transport of aerosol.

For the voyage data, Figure 4d-g, the control run shows a general underestimation of CCN compared to the observations in  
425 all seasons and regions with a robust sample size. The results for the summer months in the northern-most latitudes have the best accuracy, 17% underestimated, although again we note a small sample size for these statistics. For the remaining regions, all seasons are more strongly underestimated, with summer generally the strongest (58%, 63% and 69% for the mid-latitudes, sub-polar and polar regions). Autumn in the mid-latitudes is approximately 42% underestimated, with the remaining seasons and regions having too few data points.

430 For the experimental simulations, at KCG, the BL NPF simulation (light red) results in a large increase in CCN in the summer (peak in February) and spring (peak in October), with little change in the early winter months, indicating a strong signal likely due to biogenic activity. This strong signal is not as pronounced as that of the N10, the comparison of which will be discussed in the next section. For MI, turning on BL NPF has only a small effect on these larger sized particles, underestimating observed CCN concentrations by 54% (compared to 59% in the control). Similarly, for Syowa, despite no observations to compare with,  
435 we can see that turning on BL NPF does not greatly impact the CCN concentrations compared to the control simulation. For the voyage data, the largest effect of the BL NPF is found in the northern most latitudes.

Turning on PMO has a greater impact on CCN, resulting in more CCN40 sized particles across all stations and voyage data with a robust sample size. The PMO simulation makes a strong contribution towards improving the MI CCN concentrations from 59% underestimated in the control to 48%, while at KCG, it increases the overestimation by 3%. For the voyage data, the



440 PMO reduces the overall bias from 17% underestimated to 2% overestimated in the northern region, from 49% to 33% in the mid-latitudes region, from 64% to 47% in the sub-polar region and from 71% to 60% in the polar region.

The three changes to the DMS climatology have a much reduced impact on the CCN compared to the previous perturbations. For the Control\* simulations, the annual CCN concentrations are similar to the control, with some seasonal variation. For the OM2 DMS climatology, across all stations and voyages we see a general reduction in CCN throughout the year, again  
445 indicating that this climatology is not fit for purpose. For the H22 DMS, the CCN concentrations are generally similar to the control throughout the year in terms of seasonal cycle and magnitude. In spring we see marginally increased CCN in the station and voyage data.

Increasing the SSA flux led to large increases in CCN at MI, where in the control, CCN was underestimated by 59%, but is only 20% below the observed in the SSA run. This increase in CCN (approximately 2 x) is inline with that suggested by  
450 Regayre et al. (2020). However, we note that the region of interest in Regayre et al. (2020) is south of MI, where less differences are found. The largest increases at MI are found during the winter. For the other stations, increases in CCN are also found but not of the scale as that seen at MI. KCG is overestimated by 30%. At Syowa the annual median increased from  $18 \text{ cm}^{-3}$  to  $25 \text{ cm}^{-3}$  (noting no observations to compare against at this location). For the voyage data, the SSA gust simulation generally improves the CCN representation, especially in the mid-latitude and sub-polar regions summer and autumn Figure 4e-f.

455 In the PMO+H22 simulation, an improvement in CCN compared to the control simulation is found for all stations and voyages. It provides a smaller increase in CCN compared to the PMO only simulation in most marine regions (eg. at MI the bias is only reduced by 3% for PMO+H22, compared to 10% for PMO only), and reduced the CCN overestimation at KCG to just 6%. We suggest that these differences likely reflect the reduced scaling of the H22 DMS climatology from 1.7 to 1.0. We note that the H22 climatology (scaled by 1.7) compared to the Lana climatology in the control (also scaled by 1.7) was found  
460 to have little impact on over all CCN concentrations. By scaling the DMS emissions back to 1.0, precursor gases are reduced potentially lowering the number of aerosol available to grow, or reducing the volume of condensable vapours to grow small aerosol particles to CCN sizes. This finding demonstrates the importance of considering a system as a whole, where different aerosol sources can impact upon the potential of others to grow to climate relevant sizes. In the Southern Ocean and Antarctic in particular, with the abundance of natural aerosol, the interplay and regional dominance between primary and secondary  
465 aerosol is only just being explored in observations.

### 4.3 CCN/N10 activation ratios

To bring the results of N10 and CCN into context, we now look at the activation ratios derived from the two aerosol size ranges, shown in Figure 5. Activation ratios, where CCN is divided by the N10 concentration are a measure of what fraction of the aerosol population can activate to be of relevance to clouds and radiation. A larger activation ratio indicates that most N10 can  
470 serve as CCN, indicating a larger sized population (larger Aitken and accumulation mode). Lower activation ratios can indicate a smaller sized population (nucleation or Aitken mode). As well as giving information about the size of the aerosol population, activation ratios can provide some information about the composition (Mallet et al., 2017). Activation ratios are useful to look at when aerosol size distributions are not available.

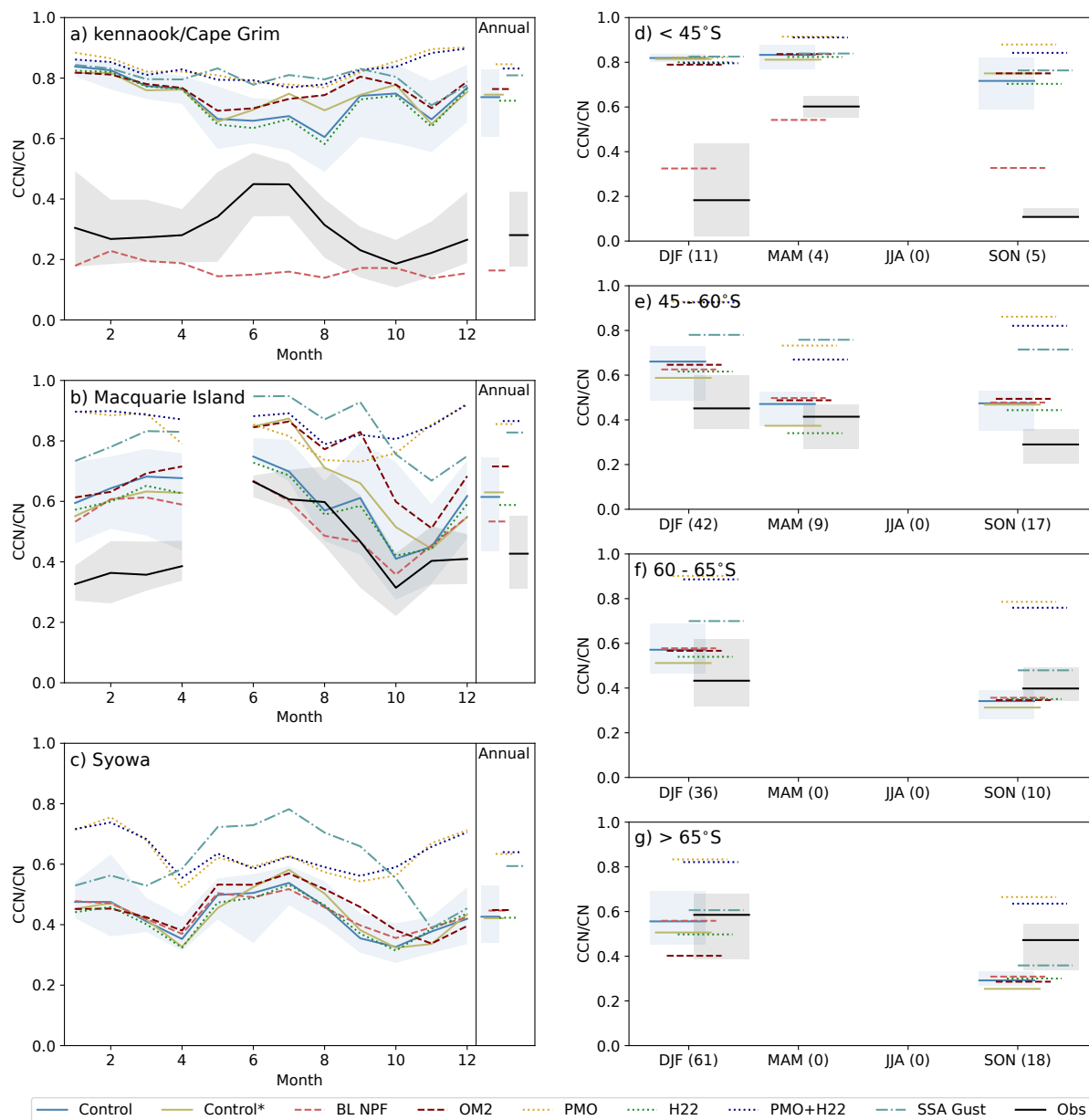


**Figure 5.** The monthly and annual median activation ratios (CCN<sub>40</sub>/N<sub>10</sub>) for at (a) kennaook/Cape Grim, (b) Macquarie Island and (c) Syowa and the seasonal medians for voyage data by latitude (d) north of 45°S, (e) 45–60°S, (f) 60–65°S and (g) south of 65°S. For all, the 25th and 75th percentiles are shown by the shaded range for the observations and control run. The observations are shown in black, while each of the model simulations are shown in colour including the control (blue), BL NPF (light red), H22 DMS (green), OM2 DMS (dark red), PMO (yellow), PMO + H22 (navy) and SSA Gust (teal). We note that there are no CCN observations available for Syowa and hence no observed ratio, similarly there are no concurrent days of N<sub>10</sub> and CCN at Macquarie Island for the month of May.



For KCG (Figure 5) lower observed activation ratios during the warmer months indicate the presence of secondary aerosols  
475 being formed from precursor gases into the smaller modes (Humphries et al., 2023). In the cooler months, the lack of these  
precursor gases results in a larger population size dominated by sea spray giving a higher activation ratio. In comparison, each  
of the model runs present a relatively flat seasonal cycle of activation ratio, missing entirely the wintertime peak. The larger  
activation ratio in the control run compared to the observations reflects the significant underestimation of the smaller sized  
N10 particles, compared to the CCN which was better captured, although overestimated. For MI, the activation ratio is also  
480 overestimated by the control. The control simulation does show a more well-defined seasonal cycle and is within the range  
of observed variability in the second half of the year. The largest (wintertime) ratios in the control and observations indicate  
a change of influence from secondary aerosol sources to primary sources such as sea spray. We note that although during  
winter months at MI the model does not reproduce the wintertime peak in CCN, compared to the observed, the activation ratio  
seasonal shape remains somewhat consistent with the observed. This further suggests inconsistencies between the observations  
485 and model. Finally, for the voyage data with a robust sample size (primarily summertime), the activation ratios for the control  
run compared to the observations is in most cases overestimated, except for in the high latitudes where it is underestimated.

For the experimental simulations, for both the voyage data and stations data broadly, the PMO (yellow), PMO+H22 (green)  
and SSA gust (teal) simulations have acted to increase the CCN closer to that of what is observed for most regions except  
that of KCG and the northern most voyage data. This made only a small impact on the N10, with marginal increases. This is  
490 reflected in the ratios, which have in general increased above that of the control simulation, and moved further away from the  
observed. This highlights the model's inability to correctly capture the aerosol size distribution.

Our analysis has shown that the ACCESS-AM2 model, with GLOMAP-mode, in general does a poor job of representing  
aerosol populations in the Southern Ocean, with the only exception being KCG CCN, although that is still overestimated. As  
stated above, despite improvements to the CCN (although less so for the N10) shown for some of the experiments (eg. PMO,  
495 PMO+H22 and SSA gust), we see a worsening of the activation ratios, suggesting that the aerosol scheme is not reflecting the  
reality of the Southern Ocean aerosol and the microphysical processes that govern it. One way to better diagnose these biases  
would be with a comparison to size distribution data, however, observed size distributions are available only for a few individual  
ship campaigns, and not for the stations of interest during this time period. An analysis of modelled aerosol size distribution  
compared to observations is planned on a large scale basis such as in this study once more observations are available. There is  
500 also work underway exploring individual campaigns.

## 5 Impacts on radiative forcing

A number of the experiments presented in this work have made a small but generally positive impact on the CCN (less so  
for the N10) for the marine and Antarctic regions studied. Before we can recommend their adoption for future releases of  
the model, we must consider their global impacts. In this sense, we are most interested in the impact of CCN, which are of  
505 a climatically relevant size, on the radiative balance of the Earth. As discussed in the introduction, the Southern Ocean has a  
persistent radiative bias, allowing too much sunlight to reach the surface during austral summer, in part as a result on incorrect

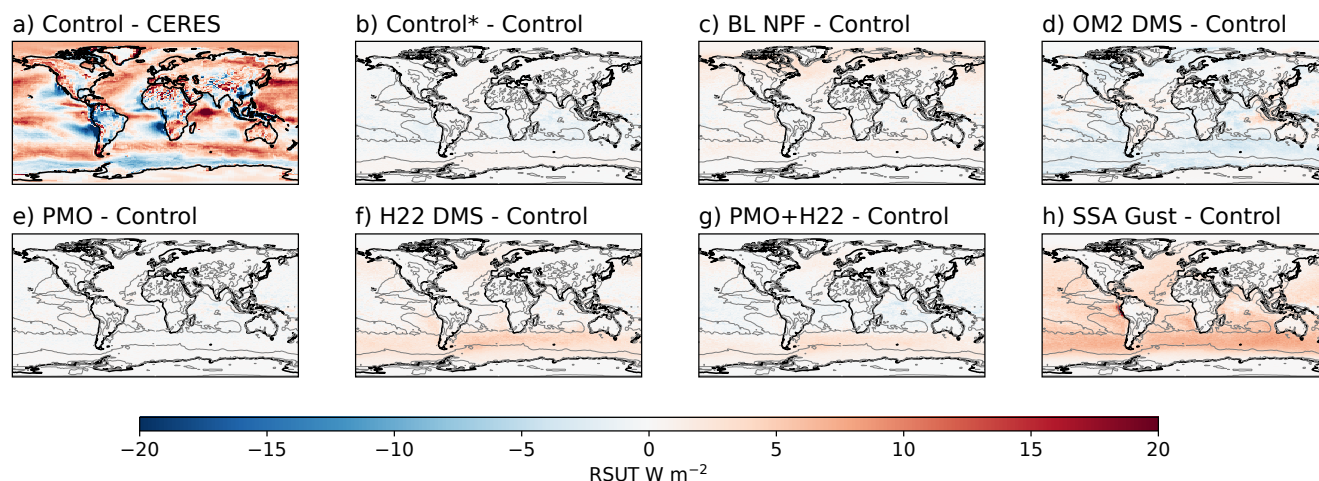


**Figure 6.** The annual mean radiative changes for the top of atmosphere shortwave upwelling radiation (RSUT) in  $\text{W m}^{-2}$  for a) the control minus the CERES satellite, and for the experimental simulations the difference from the control for: b) Control\*, c) BL NPF, d) OM2 DMS, e) PMO, f) H22 DMS, g) PMO+H22 and h) SSA gust. For plots b-h) the zero contour line of plot a) is shown to indicate where the observational bias changes sign.

partitioning of cloud phase. Significant work has previously been done to explore this radiation bias in the version of the ACCESS-AM2 model evaluated here. Fiddes et al. (2022) showed that the liquid water path in the model was significantly underestimated, while the ice water path was overestimated. Fiddes et al. (2024) further suggested, using machine learning, that improvements in the model's liquid water path would have the most impact on reducing the radiative bias. Here we explore if the improvements to CCN have resulted in changes to the radiative bias, via the liquid water path. We note that we have evaluated other cloud properties, and the aerosol direct effect via clear sky radiation, but for brevity will not discuss them here.

Figure 6 shows the annual mean shortwave up-welling top of atmosphere radiation (RSUT) bias (a), and the changes from the control simulation for each of the experiments (b-h). The contour lines represent the threshold of positive to negative observed biases (as seen in a). Table 2 shows the change in bias from the observed for the annual mean and summer time over a number of regions. We note that the regions defined in the table are not the same as those defined by Humphries et al. (2023) and used in the sections above, but match those defined in Fiddes et al. (2022) in relation to the radiative bias.

The four runs that are considered to be the 'best' in terms of improving CCN are PMO, PMO+H22 and the SSA gust simulations. Here we can see that the PMO simulation Figure 6e has little impact on the radiative bias annually, while the combined PMO+H22 (Figure 6g) simulation has a positive change over the Southern Ocean and a weakly negative change elsewhere. The annual polar region bias is reduced from  $-3.43 \text{ W m}^{-2}$  to  $-2.18 \text{ W m}^{-2}$ , while the global mean only increases by  $0.2 \text{ W m}^{-2}$ . The SSA gust simulation, despite dramatically reducing the polar region bias to  $-0.85 \text{ W m}^{-2}$ , shows an overall increase in the amount of reflected shortwave radiation mostly in regions outside of the polar region (Figure 6h), almost doubling the global radiative bias from  $2.40 \text{ W m}^{-2}$  to  $4.65 \text{ W m}^{-2}$ .



**Table 2.** Mean outgoing top of atmosphere shortwave radiation bias (from the CERES satellite) for the annual and DJF periods, over four regions: global, Southern Ocean (43-69°S), subpolar region (43-58°S) and polar regions (58-69°S), for each simulation. We have highlighted in bold the best performing (according to the mean bias) simulation for each region/season

|          | Annual      |              |             |              | DJF          |              |             |               |
|----------|-------------|--------------|-------------|--------------|--------------|--------------|-------------|---------------|
|          | Glob        | SO (43-69S)  | SP (43-58S) | P (58-69S)   | Glob         | SO (43-69S)  | SP (43-58S) | P (58-69S)    |
| Control  | 2.4         | 1.63         | 5.43        | -3.43        | 0.18         | -6.26        | 2.37        | -17.78        |
| Control* | 2.32        | 1.87         | 5.49        | -2.95        | 0.24         | -5.03        | 3.07        | -15.84        |
| BL NPF   | 2.89        | 1.94         | 5.87        | -3.3         | 0.31         | -5.76        | 3.01        | -17.45        |
| OM2      | <b>1.85</b> | <b>-0.09</b> | <b>3.64</b> | -5.06        | -0.98        | -10.93       | -2.79       | -21.78        |
| PMO      | 2.37        | 1.7          | 5.44        | -3.28        | <b>-0.03</b> | -6.54        | <b>1.76</b> | -17.62        |
| H22      | 3.19        | 4.19         | 8.58        | -1.65        | 1.33         | <b>-1.07</b> | 7.93        | -13.06        |
| PMO+H22  | 2.6         | 3.28         | 7.38        | -2.18        | 0.4          | -3.41        | 5.08        | -14.72        |
| SSA Gust | 4.65        | 6.23         | 11.54       | <b>-0.85</b> | 2.69         | 1.12         | 11.18       | <b>-12.28</b> |

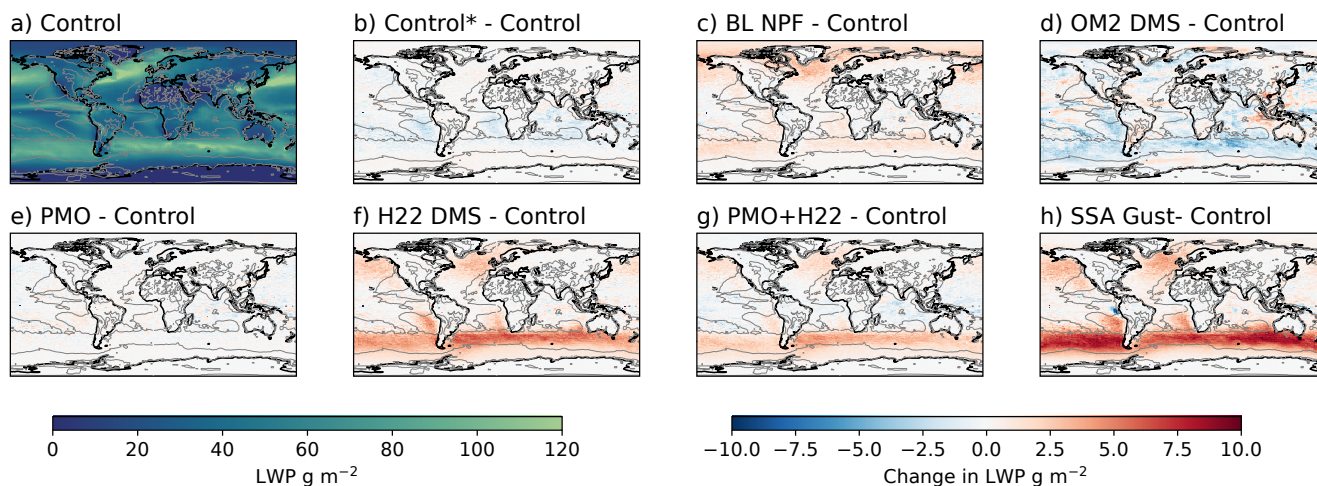


**Figure 7.** The annual mean liquid water path ( $\text{kg m}^{-2}$ ) for the Control run (a) and the annual mean difference in liquid water path between the experimental simulation and the Control run for: b) Control\*, c) BL NPF, d) OM2 DMS, e) PMO, f) H22 DMS, g) PMO+H22 and h) SSA gust. For plots b-h) the zero contour line of Figure 6a) is shown to indicate where the observational radiative bias changes sign.

525 Figure 7 shows the liquid water path for the Control simulation and the subsequent differences from this for the experimental simulations. The changes in the annual mean shortwave radiative bias are clearly closely linked to the changes found in liquid water path, with the strongest increases over the northern parts of Southern Ocean for the SSA and H22 simulations of approximately 7.3% and 4.5% respectively. Increased liquid water results in clouds that are more optically thick, reflecting

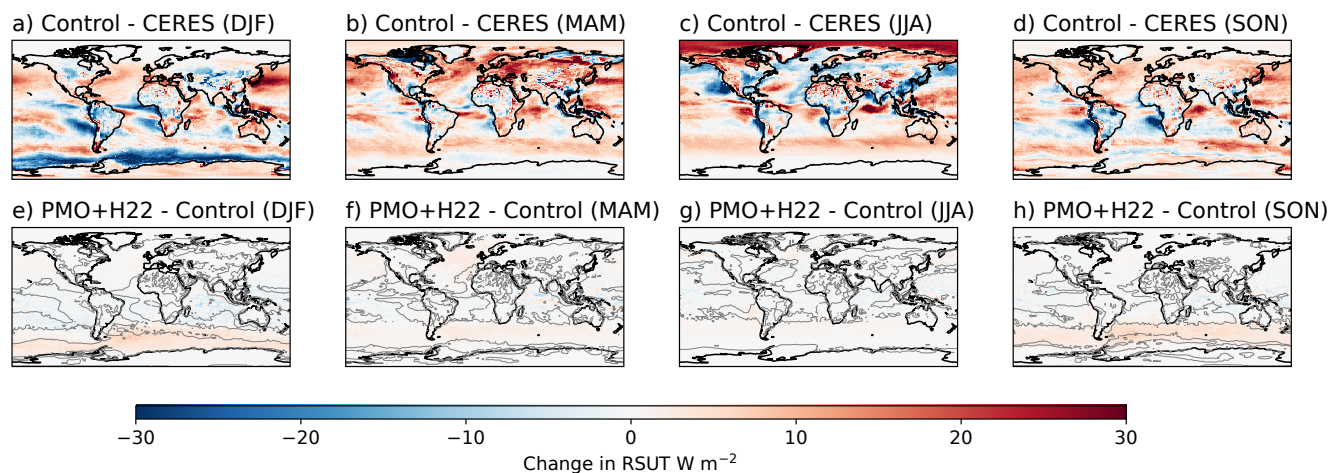


**Figure 8.** The radiative changes for the top of atmosphere shortwave upwelling radiation (RSUT) in  $\text{W m}^{-2}$  for each season (DJF, MAM, JJA, SON from left to right) for the control minus the CERES satellite (top) and for the PMO+H22 experiment minus the control (bottom). For plots e-h) the zero contour line of plots a-d) are shown to indicate where the observational bias changes sign.

more radiation back out to space. Similar responses were found for the liquid cloud fraction (an overall increase, though weaker  
530 in relative terms), while insignificant positive changes were found for the ice water path (not shown).

If we consider the seasonal breakdown of the PMO+H22 simulation only (Figure 8) we can see a clear improvement of the summertime polar Southern Ocean negative radiative bias, going from  $-17.78 \text{ W m}^{-2}$  to  $-14.72 \text{ W m}^{-2}$ , with a degradation of the positive bias in the northern region of the Southern Ocean ( $2.37 \text{ W m}^{-2}$  to  $5.08 \text{ W m}^{-2}$ ). Autumn (MAM) and winter (JJA) season see little to no change in the top of atmosphere radiation, while we can see a positive change in spring (SON).

## 535 6 Discussion

The impact of the changes in aerosol on the radiation budget raises a few important discussion points. Firstly, the small increase in outgoing shortwave radiation annually as a result of the H22 DMS climatology, particularly over the Southern Ocean, indicates that even a small improvement in the representation of biologically derived aerosol sources can have a meaningful impact on the global radiation budget. Combining H22 with PMO, another biologically derived aerosol source, constrains the  
540 increase in SW top of atmosphere radiation even further to the region of largest bias, reinforcing this idea. It also demonstrates the internal complexity of the aerosol population and the need to consider it as a whole, rather than as individual (compositional) populations.

The inclusion of PMO and the H22 climatology only marginally improved the N10 and CCN concentrations, however they do point towards opportunity for future work. For DMS, in the ACCESS model, a mask is applied over sea ice zones, limiting the  
545 flux of DMS in accordance with the fraction of ocean covered by sea ice. However, research has shown that coastal Antarctica



and sea ice regions are very biologically active and a large potential source of DMS (Trevena and Jones, 2012; Damm et al., 2016; Webb et al., 2019). None of the DMS climatologies incorporate DMS from sea ice (Lannuzel et al., 2024) which can be a dominant source in ice-covered regions (Hayashida et al., 2020). Furthermore, in ACCESS, the surface water DMS is masked out where sea ice is found, inhibiting its potential to influence the atmospheric composition. Representing this source of sulfate  
550 aerosol in the model may lead to a further increase of N10 and CCN in this region and a reduction in the shortwave bias. We can see some evidence of this impact if we look at the results of the Control\* simulation, which, as shown, had extremely high summertime DMS concentrations in this region. The Control\* simulation had larger N10 than the control, but a lesser impact on CCN, which resulted in only a small increase in outgoing shortwave radiation in this region. This suggests that the addition of a sea ice-derived DMS source would help to reduce the region of largest bias, though would not be enough on its own to fix  
555 the problem.

A known limitation of GLOMAP-mode is that it does not represent aerosol derived from methanesulfonic acid (MSA). MSA is another product of DMS oxidation in the atmosphere, as well as sulfuric acid. In GLOMAP-mode, MSA is produced in the gas phase, but is not then considered as a contributor to the aerosol burden. Revell et al. (2019) progressed the MSA representation in the UKCA-chemistry, adding aqueous phase MSA. However this remains disconnected to the aerosol scheme  
560 to form MSA aerosol. The changes by Revell et al. (2019) are also not included in the offline-chemistry configuration of the UKCA used in this study. We suggest that adding the MSA derived aerosol to GLOMAP-mode may have some impact on increasing the aerosol burden of the Southern Ocean.

We find that BL NPF had little impact on the marine regions of the Southern Ocean and Antarctica. We suggest that this is partly due to a lack of marine derived secondary organics which, in the BL NPF scheme used, mediate the reaction. For  
565 example, recent work has shown that the Southern Ocean and biologically active sea ice regions produce significant amounts of isoprene (Ferracci et al., 2024; Rodríguez-Ros et al., 2020; Brean et al., 2021). This source is not included in the secondary organic climatologies for continental areas, let alone marine regions, in the version of GLOMAP used here, but recent work has begun to include such emissions (Ferracci et al., 2024). This again represents an area of improvement of the Southern Ocean. Isoprene and other secondary organics are further limited to just condensational sources within GLOMAP-mode, without the  
570 capability of forming aerosol themselves.

While including a marine source of secondary organics in GLOMAP mode may increase BL NPF for Southern Ocean regions, there remains a question about the reality of how much BL NPF actually occurs (not much according to Brean et al., 2021; Schmale et al., 2019). Recent campaigns near the Antarctic coastline indicate that a large amount of the secondary aerosol is in fact coming from long range transport over the Antarctic continent (McCoy et al., 2021; Mace et al., 2024), not  
575 particles formed in-situ. It is suggested that sulfuric acid sourced from these biologically active regions is lofted into the free troposphere where it can easily undergo new particle formation and growth. It is then circulated over the continent, where subsidence and katabatic outflow occur, transporting sulfate aerosol to the coastal regions at large, climatically relevant sizes. Along the coastline, a lack of precipitating clouds helps retain high CCN numbers. This long-range transport of biologically derived aerosol, involving both microphysical and dynamical processes, is a crucial source of high CCN numbers in coastal



580 Antarctic regions. To date, no study has evaluated whether an atmospheric model can replicate both the aerosol formation and long-range transport mechanisms suggested in the observations.

Finally, with respect to biologically derived aerosol, our experiments show that it is the addition of PMO that really drives the increase of CCN, by providing Aitken mode sized surfaces upon which precursor gases can condensed and grow. Currently in ACCESS the PMO is derived from a fractional assumption of the sea spray using chlorophyll-a as the reference for biological activity. A recent review has suggested that chlorophyll-a may not be a good general proxy for organics (Russell et al., 2023). Furthermore, the assumption that all PMO is released into the Aitken mode (as is currently done) may also be an oversimplification of this process (Quinn et al., 2015; Prather et al., 2013).

While the changes in radiative forcing is small as a result of PMO here, we must also consider its potential impact on cloud phase. PMO is a source of ice nucleating particle, and significant effort globally is being undertaken to link INP directly to cloud schemes, instead of using empirical temperature based parameterisations. These efforts rely on the accurate representation of aerosol composition and highlights the need for comprehensive compositional data for model development, as shown in McCluskey et al. (2023). In the next generation of ACCESS models, which should include new double moment microphysics (Field et al., 2023), we hope to be able to make this direct connection from aerosol to cloud phase.

Overall, small improvements to the CCN as a result of improving biologically derived aerosol representation has helped the summer time radiative bias, albeit with some adverse effects errors in spring. This does suggest however that if we do more to better represent the biological cycle in our climate models, we may have a better chance of simulating the aerosol-climate system.

On the other hand, our experiments using SSA derived from the wind gusts show significant improvements in CCN over the mid-latitude ranges of the Southern Ocean. While the improvement in CCN was intended, it also resulted in a significant degradation of the shortwave radiation bias for the region (the bias becomes more positive). While a positive change is desirable further south of Macquarie Island (where the bias is negative), to the north of this region, a positive change results in a larger positive bias. This is particularly concerning as this region has been highlighted as an area of large uncertainty when it comes to cloud feedbacks (Zelinka et al., 2020), and aerosol-cloud interaction is understood to be one of the most uncertain components of this. We also note that the opposite is also true, where the simulations with the largest aerosol number concentration biases (OM2) reflects the smallest radiative bis annually outside of the polar region.

These results point to at least two possible conclusions. The first is that the model has been so highly tuned that the improvement of the physical representation of particular components results in a worsening of downstream systems. The second is that the biases in CCN in the model have been masking potentially even worse biases within the cloud scheme, and by improving the aerosol representation, we are revealing these errors. In reality, it is likely that these two hypotheses are inextricably linked and points to a need to consider model development in this space as an entire system rather than individual components. However, this task in itself is, as one might say, enormous.



## 7 Conclusions

The Southern Ocean aerosol population has been shown here to be poorly simulated by a sophisticated double moment aerosol scheme, GLOMAP-mode, within the ACCESS-AM2 framework. N10 aerosol are significantly underestimated in all regions examined. Outside of continental Australian influences, larger CCN sized aerosol numbers are also significantly underestimated. Our attempts to increase these populations have been limited in success. To summarise, turning on BL NPF significantly increases N10 only in Australian continental influenced regions, having little impact on either N10 or CCN in other regions. The use of a time varying, parameterised DMS climatology resulted in reductions in aerosol number, indicating that the parameterisation used is not suitable for this region. Updating the DMS climatology to the new H22 dataset made only small differences to aerosol number. However scaling back the DMS flux parameter to 1.0 (instead of 1.7) and adding PMO increased CCN whilst also decreasing N10. Turning on PMO alone showed larger increases in CCN, possibly resulting from faster growth to larger sized aerosol. Finally, increasing the SSA flux in line with wind gusts instead of mean wind speed significantly increased CCN in the marine regions, particularly in winter.

Our results have demonstrated issues with capturing the size and number of aerosol populations, and points towards missing aerosol sources and possibly issues within the aerosol scheme structure or microphysics. We reiterate a strong need for comprehensive aerosol observations in the Southern Ocean region to inform model development, including size and compositional information.

From our experiments, we suggest that future versions of ACCESS do consider using the H22 DMS climatology, with emissions scaled to 1.0, in combination with the PMO turned on. Switching on PMO and re-scaling DMS brings ACCESS inline with more recent versions of the UM global atmosphere configurations, while the H22 data-set represents the newest knowledge in terms of DMS concentrations.

The impacts of these changes on the radiative balance have also been investigated. The H22+PMO combined experiment yielded the best results as far as improving the Southern Ocean radiative bias, whilst having limited adverse effects constrained to the northern parts of the Southern Ocean in springtime. The SSA gust experiment had the largest impact, increasing the amount of sunlight reflected out to space across the globe, with large, undesirable effects on regions outside of the Southern Ocean. This result is of particular concern given that large improvements to the CCN has resulted in untenable increase of the radiative bias in the northern latitudes of the Southern Ocean. Such an outcome poses a challenge for all in the earth system modelling community.

*Code and data availability.* All model data is hosted on Zenodo at <https://doi.org/10.5281/zenodo.13864183>. Code for this project is provided on GitHub via [https://github.com/sfiddes/ACCESS\\_aerosol\\_eval](https://github.com/sfiddes/ACCESS_aerosol_eval). CN and CCN data from Macquarie Island are available at <https://doi.org/10.25919/g7jx-k629> (Humphries et al., 2021b). Data from kennaook / Cape Grim are available at the World Data Centre for Aerosols at <https://ebas-data.nilu.no> (Keywood et al., 2023a, b). Syowa data are available at <https://doi.org/10.17592/002.2023030399> (Hara, 2023). Data from MARCUS are available at <https://doi.org/10.25919/ezp0-em87> (Humphries, 2020). Cold Water Trial data are available at <https://doi.org/10.25919/ytsw-9610> (Humphries et al., 2022b). CAPRICORN1 data are available at <https://doi.org/10.25919/5f688fcc97166>



645 (Protat, 2020). Ice2Equator data are available at <https://doi.org/10.25919/g07r-b187> (Humphries et al., 2022a). PCAN data are available  
at <https://doi.org/10.25919/xs0b-an24> (Humphries et al., 2020b). CAPRICORN2 data are available at <https://doi.org/10.25919/2h1c-t753>  
(Humphries et al., 2020a). CAMMPCAN data are available at <http://dx.doi.org/doi:10.26179/5e546f452145d> (Schofield and Ryan, 2021).

*Author contributions.* SF has performed the analysis, writing and model runs. MW provided advice and assistance with the model runs. RH  
led the collection and quality control for the ship-based aerosol observations presented here, and was involved in the collation the remainder  
650 of the observations used. MM has provided expert advise on observed aerosol characteristics and experimental setup. This study has expanded  
upon LL's honours thesis (supervised by SF, MW and RH), which provided an initial concept of this study. SP and AP have provided guidance  
throughout this study. HH developed the OM2 DMS dataset. BM, SP, RH and RS provided the quality controlled CAMMPCAN observations,  
and RS additional compute resources. All authors have contributed to the revisions of this manuscript.

*Competing interests.* The authors declare that they have no competing interests

655 *Acknowledgements.* We would like to thank the useful discussions with Peter May which led to the changes in the sea spray flux parameteri-  
sation. This project received grant funding from the Australian Government as part of the Antarctic Science Collaboration Initiative program,  
under the Australian Antarctic Program Partnership, ASCI000002. Resources and services from the National Computational Infrastructure  
(Project jk72, gx60, v45 and q90), supported by the Australian Government, were used. S.F. acknowledges the Australian Research Coun-  
cil Centre of Excellence for Climate Extremes and the Australian Earth System Simulator National Research Infrastructure, funded by the  
660 Australian Government's National Collaborative Research Infrastructure Strategy, for their maintenance of virtual environments, code and  
model support. The authors would like to acknowledge the teams at NASA CERES for making the radiation data used in this work publicly  
available. The Authors wish to thank the CSIRO Marine National Facility (MNF) for its support in the form of sea time on RV Investigator,  
support personnel, scientific equipment and data management. All data and samples acquired on the voyage are made publicly available  
in accordance with MNF Policy. We would also like to thank the teams at kennaook/Cape Grim, led by Melita Keyword, and the Korean  
665 station Syowa, led by Keiichiro Hara, for their work in producing the datasets used here. Technical and logistical support for the deploy-  
ment to Macquarie Island were provided by the Australian Antarctic Division through Australian Antarctic Science Project 4292, and we  
thank George Brettingham-Moore, Ken Barrett, Nick Cartwright, Nick Cole (deceased), Emry Crocker, Terry Egan, John French, Eric King  
(deceased), Ian McRobert, Lloyd Symons, Peter de Vries and Steven Whiteside for all of their assistance. Technical and logistical support  
for the deployment of CAMMPCAN on the RSV Aurora Australis 2017-2018 and 2018-2019 by the Australian Antarctic Division through  
670 Australian Antarctic Science Project 4431. AIRBOX was funded by the Australian Research Council LIEF grant: LE150100048.



## References

- Albrecht, B. A.: Aerosols, cloud microphysics, and fractional cloudiness., *Science*, 245, 1227–1230, <https://doi.org/10.1126/science.245.4923.1227>, 1989.
- Alroe, J., Cravigan, L. T., Miljevic, B., Johnson, G. R., Selleck, P., Humphries, R. S., Keywood, M. D., Chambers, S. D., Williams, A. G., and Ristovski, Z. D.: Marine productivity and synoptic meteorology drive summer-time variability in Southern Ocean aerosols, *Atmospheric Chemistry and Physics*, 20, 8047–8062, <https://doi.org/10.5194/acp-20-8047-2020>, 2020.
- Aranami, K. and Tsunogai, S.: Seasonal and regional comparison of oceanic and atmospheric dimethylsulfide in the northern North Pacific: Dilution effects on its concentration during winter, *Journal of Geophysical Research D: Atmospheres*, 109, <https://doi.org/10.1029/2003JD004288>, 2004.
- Bell, T. G., Landwehr, S., Miller, S. D., De Bruyn, W. J., Callaghan, A. H., Scanlon, B., Ward, B., Yang, M., and Saltzman, E. S.: Estimation of bubble-mediated air-sea gas exchange from concurrent DMS and CO<sub>2</sub> transfer velocities at intermediate-high wind speeds, *Atmospheric Chemistry and Physics*, 17, 9019–9033, <https://doi.org/10.5194/acp-17-9019-2017>, 2017.
- Bhatti, Y. A., Revell, L. E., Schuddeboom, A. J., McDonald, A. J., Archibald, A. T., Williams, J., Venugopal, A. U., Hardacre, C., Behrens, E., and Bhatti, Y.: The sensitivity of Southern Ocean atmospheric dimethyl sulfide to modelled sources and emissions, *ACPD*, <https://doi.org/10.5194/egusphere-2023-868>, 2023.
- Bi, D., Dix, M., Marsland, S., O’Farrell, S., Sullivan, A., Bodman, R., Law, R., Harman, I., Srbinovsky, J., Rashid, H. A., Dobrohotoff, P., Mackallah, C., Yan, H., Hirst, A., Savita, A., Dias, F. B., Woodhouse, M., Fiedler, R., and Heerdegen, A.: Configuration and spin-up of ACCESS-CM2, the new generation Australian Community Climate and Earth System Simulator Coupled Model, *Journal of Southern Hemisphere Earth Systems Science*, 70, 225–251, <https://doi.org/10.1071/es19040>, 2020.
- Bock, J., Michou, M., Nabat, P., Abe, M., Mulcahy, J. P., Olivić, D. J. L., Schwinger, J., Suntharalingam, P., Tjiputra, J., van Hulten, M., Watanabe, M., Yool, A., and Séférian, R.: Evaluation of ocean dimethylsulfide concentration and emission in CMIP6 models, *Biogeosciences*, 18, 3823–3860, <https://doi.org/10.5194/bg-18-3823-2021>, 2021.
- Bodas-Salcedo, A., Williams, K. D., Ringer, M. A., Beau, I., Cole, J. N. S., Dufresne, J. L., Koshiro, T., Stevens, B., Wang, Z., and Yokohata, T.: Origins of the solar radiation biases over the Southern Ocean in CFMIP2 models, *Journal of Climate*, 27, 41–56, <https://doi.org/10.1175/JCLI-D-13-00169.1>, 2014.
- Bodman, R. W., Karoly, D. J., Dix, M. R., Harman, I. N., Srbinovsky, J., Dobrohotoff, P. B., and Mackallah, C.: Evaluation of CMIP6 AMIP climate simulations with the ACCESS-AM2 model, *Journal of Southern Hemisphere Earth Systems Science*, 70, 166–179, <https://doi.org/10.1071/ES19033>, 2020.
- Boucher, O., Randall, D., Artaxo, P., Bretherton, C., Feingold, G., Forster, P., Kerminen, V. M., Kondo, Y., Liao, H., Lohmann, U., Rasch, P., Satheesh, S. K., Sherwood, S., Stevens, B., Zhang, X. Y., and Zhan, X. Y.: Clouds and Aerosols, in: *Climate Change 2013: The Physical Science Basis. Contribution of Working Group I to the Fifth Assessment Report of the Intergovernmental Panel on Climate Change*, edited by Stocker, T., Qin, D., Plattner, G.-K., Tignor, M., Allen, S., Boschung, J., Nauels, A., Xia, Y., Bex, V., and Midgley, P., pp. 571–657, Cambridge University Press, Cambridge, United Kingdom and New York, NY, USA, <https://doi.org/10.1017/CBO9781107415324.016>, 2013.
- Brean, J., Dall’Osto, M., Simó, R., Shi, Z., Beddows, D. C. S., and Harrison, R. M.: Open ocean and coastal new particle formation from sulfuric acid and amines around the Antarctic Peninsula, *Nature Geoscience*, <https://doi.org/10.1038/s41561-021-00751-y>, 2021.



- Burrows, S. M., McCluskey, C. S., Cornwell, G., Steinke, I., Zhang, K., Zhao, B., Zawadowicz, M., Raman, A., Kulkarni, G., China, S., Zelenyuk, A., and DeMott, P. J.: Ice-Nucleating Particles That Impact Clouds and Climate: Observational and Modeling Research Needs, <https://doi.org/10.1029/2021RG000745>, 2022.
- 710 Carslaw, K. S., Lee, L. A., Reddington, C. L., Pringle, K. J., Rap, A., Forster, P. M., Mann, G. W., Spracklen, D. V., Woodhouse, M. T., Regayre, L. a., and Pierce, J. R.: Large contribution of natural aerosols to uncertainty in indirect forcing., *Nature*, 503, 67–71, <https://doi.org/10.1038/nature12674>, 2013.
- Curtius, J.: Nucleation of atmospheric aerosol particles, <https://doi.org/10.1016/j.crhy.2006.10.018>, 2006.
- Damm, E., Nomura, D., Martin, A., Dieckmann, G. S., and Meiners, K. M.: DMSP and DMS cycling within Antarctic sea ice during the winter–spring transition, *Deep-Sea Research Part II: Topical Studies in Oceanography*, 131, 150–159, <https://doi.org/10.1016/j.dsr2.2015.12.015>, 2016.
- 715 De Leeuw, G., Andreas, E. L., Anguelova, M. D., Fairall, C. W., Lewis, E. R., O’Dowd, C., Schulz, M., and Schwartz, S. E.: Production flux of sea spray aerosol, *Reviews of Geophysics*, 49, <https://doi.org/10.1029/2010RG000349>, 2011.
- Doelling, D. R., Loeb, N. G., Keyes, D. F., Nordeen, M. L., Morstad, D., Nguyen, C., Wielicki, B. A., Young, D. F., and Sun, M.: Geostationary enhanced temporal interpolation for ceres flux products, *Journal of Atmospheric and Oceanic Technology*, 30, 1072–1090, <https://doi.org/10.1175/JTECH-D-12-00136.1>, 2013.
- 720 Doelling, D. R., Sun, M., Nguyen, L. T., Nordeen, M. L., Haney, C. O., Keyes, D. F., and Mlynyczak, P. E.: Advances in geostationary-derived longwave fluxes for the CERES synoptic (SYN1deg) product, *Journal of Atmospheric and Oceanic Technology*, 33, 503–521, <https://doi.org/10.1175/JTECH-D-15-0147.1>, 2016.
- 725 Eyring, V., Bony, S., Meehl, G. A., Senior, C. A., Stevens, B., Stouffer, R. J., and Taylor, K. E.: Overview of the Coupled Model Intercomparison Project Phase 6 (CMIP6) experimental design and organization, *Geoscientific Model Development*, 9, 1937–1958, <https://doi.org/10.5194/gmd-9-1937-2016>, 2016.
- Feng, L., Smith, S. J., Braun, C., Crippa, M., Gidden, M. J., Hoesly, R., Klimont, Z., Van Marle, M., Van Den Berg, M., and Van Der Werf, G. R.: The generation of gridded emissions data for CMIP6, *Geoscientific Model Development*, 13, 461–482, <https://doi.org/10.5194/gmd-13-461-2020>, 2020.
- 730 Ferracci, V., Weber, J., Bolas, C. G., Robinson, A. D., Tummon, F., Rodríguez-Ros, P., Cortés-Greus, P., Baccharini, A., Jones, R. L., Galí, M., Simó, R., Schmale, J., and Harris, N. R. P.: Atmospheric isoprene measurements reveal larger-than-expected Southern Ocean emissions, *Nature Communications*, 15, 2571, <https://doi.org/10.1038/s41467-024-46744-4>, 2024.
- Fiddes, S. L., Woodhouse, M. T., Nicholls, Z., Lane, T. P., and Schofield, R.: Cloud, precipitation and radiation responses to large perturbations in global dimethyl sulfide, *Atmospheric Chemistry and Physics*, 18, 10 177–10 198, <https://doi.org/10.5194/acp-18-10177-2018>, 2018.
- 735 Fiddes, S. L., Protat, A., Mallet, M. D., Alexander, S. P., and Woodhouse, M. T.: Southern Ocean cloud and shortwave radiation biases in a nudged climate model simulation: does the model ever get it right?, *Atmospheric Chemistry and Physics*, 22, 14 603–14 630, <https://doi.org/10.5194/acp-22-14603-2022>, 2022.
- 740 Fiddes, S. L., Mallet, M. D., Protat, A., Woodhouse, M. T., Alexander, S. P., and Furtado, K.: A machine learning approach for evaluating Southern Ocean cloud radiative biases in a global atmosphere model, *Geoscientific Model Development*, 17, 2641–2662, <https://doi.org/10.5194/gmd-17-2641-2024>, 2024.



- Field, P. R., Hill, A., Shipway, B., Furtado, K., Wilkinson, J., Miltenberger, A., Gordon, H., Grosvenor, D. P., Stevens, R., and Van Weverberg, K.: Implementation of a double moment cloud microphysics scheme in the UK met office regional numerical weather prediction model, Quarterly Journal of the Royal Meteorological Society, <https://doi.org/10.1002/qj.4414>, 2023.
- Forster, P., T. Storelvmo, K. Armour, W. Collins, J.-L. Dufresne, D. Frame, D.J. Lunt, T. Mauritsen, M.D. Palmer, M. Watanabe, M. Wild, and H. Zhang: The Earth's Energy Budget, Climate Feedbacks and Climate Sensitivity, in: Climate Change 2021 – The Physical Science Basis, pp. 923–1054, Cambridge University Press, <https://doi.org/10.1017/9781009157896.009>, 2023.
- Fossum, K. N., Ovadnevaite, J., Ceburnis, D., Dall'Osto, M., Marullo, S., Bellacicco, M., Simó, R., Liu, D., Flynn, M., Zuend, A., and O'Dowd, C.: Summertime Primary and Secondary Contributions to Southern Ocean Cloud Condensation Nuclei, Scientific Reports, 8, 13 844, <https://doi.org/10.1038/s41598-018-32047-4>, 2018.
- Fricko, O., Havlik, P., Rogelj, J., Klimont, Z., Gusti, M., Johnson, N., Kolp, P., Strubegger, M., Valin, H., Amann, M., Ermolieva, T., Forsell, N., Herrero, M., Heyes, C., Kindermann, G., Krey, V., McCollum, D. L., Obersteiner, M., Pachauri, S., Rao, S., Schmid, E., Schoepp, W., and Riahi, K.: The marker quantification of the Shared Socioeconomic Pathway 2: A middle-of-the-road scenario for the 21st century, Global Environmental Change, 42, 251–267, <https://doi.org/10.1016/j.gloenvcha.2016.06.004>, 2017.
- Galí, M., Levasseur, M., Devred, E., Simó, R., and Babin, M.: Sea-surface dimethylsulfide (DMS) concentration from satellite data at global and regional scales, Biogeosciences, 15, 3497–3519, <https://doi.org/10.5194/bg-15-3497-2018>, 2018.
- Gantt, B., Meskhidze, N., Facchini, M. C., Rinaldi, M., Ceburnis, D., and O'Dowd, C. D.: Wind speed dependent size-resolved parameterization for the organic mass fraction of sea spray aerosol, Atmospheric Chemistry and Physics, 11, 8777–8790, <https://doi.org/10.5194/acp-11-8777-2011>, 2011.
- Gantt, B., Johnson, M. S., Meskhidze, N., Sciare, J., Ovadnevaite, J., Ceburnis, D., and O'Dowd, C. D.: Model evaluation of marine primary organic aerosol emission schemes, Atmospheric Chemistry and Physics, 12, 8553–8566, <https://doi.org/10.5194/acp-12-8553-2012>, 2012.
- Gidden, M. J., Riahi, K., Smith, S. J., Fujimori, S., Luderer, G., Kriegler, E., Van Vuuren, D. P., Van Den Berg, M., Feng, L., Klein, D., Calvin, K., Doelman, J. C., Frank, S., Fricko, O., Harmsen, M., Hasegawa, T., Havlik, P., Hilaire, J., Hoesly, R., Horing, J., Popp, A., Stehfest, E., and Takahashi, K.: Global emissions pathways under different socioeconomic scenarios for use in CMIP6: A dataset of harmonized emissions trajectories through the end of the century, Geoscientific Model Development, 12, 1443–1475, <https://doi.org/10.5194/gmd-12-1443-2019>, 2019.
- Gong, S. L.: A parameterization of sea-salt aerosol source function for sub- and super-micron particles, Global Biogeochemical Cycles, 17, n/a–n/a, <https://doi.org/10.1029/2003GB002079>, 2003.
- Gordon, H., Sengupta, K., Rap, A., Duplissy, J., Frege, C., Williamson, C., Heinritzi, M., Simon, M., Yan, C., Almeida, J., Tröstl, J., Nieminen, T., Ortega, I. K., Wagner, R., Dunne, E. M., Adamov, A., Amorim, A., Bernhammer, A.-K., Bianchi, F., Breitenlechner, M., Brilke, S., Chen, X., Craven, J. S., Dias, A., Ehrhart, S., Fischer, L., Flagan, R. C., Franchin, A., Fuchs, C., Guida, R., Hakala, J., Hoyle, C. R., Jokinen, T., Junninen, H., Kangasluoma, J., Kim, J., Kirkby, J., Krapf, M., Kürten, A., Laaksonen, A., Lehtipalo, K., Makhmutov, V., Mathot, S., Molteni, U., Monks, S. A., Onnela, A., Peräkylä, O., Piel, F., Petäjä, T., Praplan, A. P., Pringle, K. J., Richards, N. A. D., Rissanen, M. P., Rondo, L., Sarnela, N., Schobesberger, S., Scott, C. E., Seinfeld, J. H., Sharma, S., Sipilä, M., Steiner, G., Stozhkov, Y., Stratmann, F., Tomé, A., Virtanen, A., Vogel, A. L., Wagner, A. C., Wagner, P. E., Weingartner, E., Wimmer, D., Winkler, P. M., Ye, P., Zhang, X., Hansel, A., Dommen, J., Donahue, N. M., Worsnop, D. R., Baltensperger, U., Kulmala, M., Curtius, J., and Carslaw, K. S.: Reduced anthropogenic aerosol radiative forcing caused by biogenic new particle formation, Proceedings of the National Academy of Sciences, 113, 12 053–12 058, <https://doi.org/10.1073/pnas.1602360113>, 2016.



- 780 Gras, L. J. and Keywood, M. D.: Cloud condensation nuclei over the Southern Ocean: Wind dependence and seasonal cycles, *Atmospheric Chemistry and Physics*, 17, 4419–4432, <https://doi.org/10.5194/acp-17-4419-2017>, 2017.
- Grythe, H., Ström, J., Krejci, R., Quinn, P., and Stohl, A.: A review of sea-spray aerosol source functions using a large global set of sea salt aerosol concentration measurements, <https://doi.org/10.5194/acp-14-1277-2014>, 2014.
- Hara, K.: Antarctic aerosol CN, <https://doi.org/https://doi.org/10.17592/002.2023030399>, 2023.
- 785 Hara, K., Osada, K., Nishita-Hara, C., and Yamanouchi, T.: Seasonal variations and vertical features of aerosol particles in the Antarctic troposphere, *Atmospheric Chemistry and Physics*, 11, 5471–5484, <https://doi.org/10.5194/acp-11-5471-2011>, 2011.
- Hara, K., Nishita-Hara, C., Osada, K., Yabuki, M., and Yamanouchi, T.: Characterization of aerosol number size distributions and their effect on cloud properties at Syowa Station, Antarctica, *Atmospheric Chemistry and Physics*, 21, 12 155–12 172, <https://doi.org/10.5194/acp-21-12155-2021>, 2021.
- 790 Hartery, S., Toohey, D., Revell, L., Sellegri, K., Kuma, P., Harvey, M., and McDonald, A. J.: Constraining the Surface Flux of Sea Spray Particles From the Southern Ocean, *Journal of Geophysical Research: Atmospheres*, 125, 1–19, <https://doi.org/10.1029/2019JD032026>, 2020.
- Hayashida, H., Carnat, G., Galí, M., Monahan, A. H., Mortenson, E., Sou, T., and Steiner, N. S.: Spatiotemporal Variability in Modeled Bottom Ice and Sea Surface Dimethylsulfide Concentrations and Fluxes in the Arctic During 1979–2015, *Global Biogeochemical Cycles*, 34, <https://doi.org/10.1029/2019GB006456>, 2020.
- 795 Hayashida, H., Jin, M., Steiner, N. S., Swart, N. C., Watanabe, E., Fiedler, R., Hogg, A. M., Kiss, A. E., Matear, R. J., and Strutton, P. G.: Ice Algae Model Intercomparison Project phase 2 (IAMIP2), *Geoscientific Model Development*, 14, 6847–6861, <https://doi.org/10.5194/gmd-14-6847-2021>, 2021.
- Hersbach, H., Bell, B., Berrisford, P., Hirahara, S., Horányi, A., Muñoz-Sabater, J., Nicolas, J., Peubey, C., Radu, R., Schepers, D., Simmons, A., Soci, C., Abdalla, S., Abellan, X., Balsamo, G., Bechtold, P., Biavati, G., Bidlot, J., Bonavita, M., Chiara, G., Dahlgren, P., Dee, D., Diamantakis, M., Dragani, R., Flemming, J., Forbes, R., Fuentes, M., Geer, A., Haimberger, L., Healy, S., Hogan, R. J., Hólm, E., Janisková, M., Keeley, S., Laloyaux, P., Lopez, P., Lupu, C., Radnoti, G., Rosnay, P., Rozum, I., Vamborg, F., Villaume, S., and Thépaut, J.: The ERA5 global reanalysis, *Quarterly Journal of the Royal Meteorological Society*, 146, 1999–2049, <https://doi.org/10.1002/qj.3803>, 2020.
- 800 Horsley, J. A., Broome, R. A., Johnston, F. H., Cope, M., and Morgan, G. G.: Health burden associated with fire smoke in Sydney, 2001 - 2013, *Medical Journal of Australia*, 208, 309–310, <https://doi.org/10.5694/mja18.00032>, 2018.
- Hoyer, S. and Hamman, J. J.: xarray: N-D labeled Arrays and Datasets in Python, *Journal of Open Research Software*, 5, <https://doi.org/10.5334/jors.148>, 2017.
- Hulswar, S., Simó, R., Galí, M., Bell, T. G., Lana, A., Inamdar, S., Halloran, P. R., Manville, G., and Mahajan, A. S.: Third revision of the global surface seawater dimethyl sulfide climatology (DMS-Rev3), *Earth System Science Data*, 14, 2963–2987, <https://doi.org/10.5194/essd-14-2963-2022>, 2022.
- 810 Humphries, R. S.: MARCUS ARM CN and CCN data reprocessed to remove ship exhaust influence. v2., <https://doi.org/https://doi.org/10.25919/ezp0-em87>, 2020.
- Humphries, R. S., McRobert, I. M., Ponsonby, W. A., Ward, J. P., Keywood, M. D., Loh, Z. M., Krummel, P. B., and Harnwell, J.: Identification of platform exhaust on the RV Investigator, *Atmospheric Measurement Techniques*, 12, 3019–3038, <https://doi.org/10.5194/amt-12-3019-2019>, 2019.





- Humphries, R. S., McRobert, I., Ward, J., Harnwell, J., and Keywood, M. D.: CAPRICORN2 - Atmospheric aerosol measurements from the RV Investigator voyage IN2018\_V01, <https://doi.org/https://doi.org/10.25919/2h1c-t753>, 2020a.
- 820 Humphries, R. S., Simmons, J. B., McRobert, I., Ward, J., Keywood, M., Chambers, S., Griffiths, A., Williams, A. G., and Wilson, S. R.: Polar Cell Aerosol Nucleation - atmospheric measurements from the RV Investigator voyage IN2017\_V01, <https://doi.org/https://doi.org/10.25919/xs0b-an24>, 2020b.
- Humphries, R. S., Keywood, M. D., Gribben, S., McRobert, I. M., Ward, J. P., Selleck, P., Taylor, S., Harnwell, J., Flynn, C., Kulkarni, G. R., Mace, G. G., Protat, A., Alexander, S. P., and McFarquhar, G.: Southern Ocean latitudinal gradients of cloud condensation nuclei, *Atmospheric Chemistry and Physics*, 21, 12 757–12 782, <https://doi.org/10.5194/acp-21-12757-2021>, 2021a.
- 825 Humphries, R. S., Ward, J., Keywood, M. D., and Alexander, S. p.: Atmospheric aerosol and Cloud Condensation Nuclei concentrations from Macquarie Island from 2016 to 2018. v2, <https://doi.org/https://doi.org/10.25919/g7jx-k629>, 2021b.
- Humphries, R. S., Alroe, J., Ristovski, Z., Keywood, M. D., Ward, J., McRobert, I., Cravigan, L., and Brown, R.: Aerosol Properties, Ice-edge to Equator voyage (IN2016\_V03): CN3 and CCN, <https://doi.org/https://doi.org/10.25919/g07r-b187>, 2022a.
- Humphries, R. S., Alroe, J., Ward, J., Keywood, M. D., McRobert, I., Cravigan, L., and Ristovsky, Z.: Aerosol Properties, Cold Water Trial voyage (IN2015\_E01): CN3 and CCN. v1., <https://doi.org/https://doi.org/10.25919/ytsw-9610>, 2022b.
- 830 Humphries, R. S., Keywood, M. D., Ward, J. P., Harnwell, J., Alexander, S. P., Klekociuk, A. R., Hara, K., McRobert, I. M., Protat, A., Alroe, J., Cravigan, L. T., Miljevic, B., Ristovski, Z. D., Schofield, R., Wilson, S. R., Flynn, C. J., Kulkarni, G. R., Mace, G. G., Mcfarquhar, G. M., Chambers, S. D., Williams, A. G., and Griffiths, A. D.: Measurement report: Understanding the seasonal cycle of Southern Ocean aerosols, *Atmospheric Chemistry and Physics*, 23, 3749–3777, <https://doi.org/10.5194/acp-23-3749-2023>, 2023.
- 835 Jaeglé, L., Quinn, P. K., Bates, T. S., Alexander, B., and Lin, J. T.: Global distribution of sea salt aerosols: New constraints from in situ and remote sensing observations, *Atmospheric Chemistry and Physics*, 11, 3137–3157, <https://doi.org/10.5194/acp-11-3137-2011>, 2011.
- Kettle, A. J., Andreae, M. O., Amouroux, D., Andreae, T. W., Bates, T. S., Berresheim, H., Bingemer, H., Boniforti, R., Curran, M. A. J., DiTullio, G. R., Helas, G., Jones, G. B., Keller, M. D., Kiene, R. P., Leck, C., Lévassieur, M., Malin, G., Maspero, M., Matrai, P., McTaggart, A. R., Mihalopoulos, N., Nguyen, B. C., Novo, A., Putaud, J. P., Rapsomanikis, S., Roberts, G., Schebeske, G., 840 Sharma, S., Simó, R., Staubes, R., Turner, S., and Uher, G.: A global database of sea surface dimethylsulfide (DMS) measurements and a procedure to predict sea surface DMS as a function of latitude, longitude, and month, *Global Biogeochemical Cycles*, 13, 399–444, <https://doi.org/10.1029/1999GB900004>, 1999.
- Keywood, M. D., Ward, J., and Derek, N.: Cloud Condensation Nuclei Number Concentration, <https://ebas-data.nilu.no/>, 2023a.
- Keywood, M. D., Ward, J., and Derek, N.: Particle Number Concentration, <https://ebas-data.nilu.no>, 2023b.
- 845 Kirkby, J., Duplissy, J., Sengupta, K., Frege, C., Gordon, H., Williamson, C., Heinritzi, M., Simon, M., Yan, C., Almeida, J., Trostl, J., Nieminen, T., Ortega, I. K., Wagner, R., Adamov, A., Amorim, A., Bernhammer, A. K., Bianchi, F., Breitenlechner, M., Brilke, S., Chen, X., Craven, J., Dias, A., Ehrhart, S., Flagan, R. C., Franchin, A., Fuchs, C., Guida, R., Hakala, J., Hoyle, C. R., Jokinen, T., Junninen, H., Kangasluoma, J., Kim, J., Krapf, M., Kurten, A., Laaksonen, A., Lehtipalo, K., Makhmutov, V., Mathot, S., Molteni, U., Onnela, A., Perakyla, O., Piel, F., Petaja, T., Praplan, A. P., Pringle, K., Rap, A., Richards, N. A., Riipinen, I., Rissanen, M. P., Rondo, L., Sarnela, N., 850 Schobesberger, S., Scott, C. E., Seinfeld, J. H., Sipila, M., Steiner, G., Stozhkov, Y., Stratmann, F., Tomé, A., Virtanen, A., Vogel, A. L., Wagner, A. C., Wagner, P. E., Weingartner, E., Wimmer, D., Winkler, P. M., Ye, P., Zhang, X., Hansel, A., Dommen, J., Donahue, N. M., Worsnop, D. R., Baltensperger, U., Kulmala, M., Carslaw, K. S., and Curtius, J.: Ion-induced nucleation of pure biogenic particles, *Nature*, 533, 521–526, <https://doi.org/10.1038/nature17953>, 2016.



- 855 Kiss, A. E., McC Hogg, A., Hannah, N., Boeira Dias, F., B Brassington, G., Chamberlain, M. A., Chapman, C., Dobrohotoff, P., Domingues, C. M., Duran, E. R., England, M. H., Fiedler, R., Griffies, S. M., Heerdegen, A., Heil, P., Holmes, R. M., Klockner, A., Marsland, S. J., Morrison, A. K., Munroe, J., Nikurashin, M., Oke, P. R., Pilo, G. S., Richet, O., Savita, A., Spence, P., Stewart, K. D., Ward, M. L., Wu, F., and Zhang, X.: ACCESS-OM2 v1.0: A global ocean-sea ice model at three resolutions, *Geoscientific Model Development*, 13, 401–442, <https://doi.org/10.5194/gmd-13-401-2020>, 2020.
- 860 Korhonen, P., Kulmala, M., Laaksonen, A., Viisanen, Y., McGraw, R., and Seinfeld, J. H.: Ternary nucleation of H<sub>2</sub>SO<sub>4</sub>, NH<sub>3</sub>, and H<sub>2</sub>O in the atmosphere, *Journal of Geophysical Research Atmospheres*, 104, 26 349–26 353, <https://doi.org/10.1029/1999jd900784>, 1999.
- Kulmala, M., Laaksonen, A., and Pirjola, L.: Parameterizations for sulfuric acid/water nucleation rates, *Journal of Geophysical Research*, 103, 8301, <https://doi.org/10.1029/97JD03718>, 1998.
- 865 Lana, A., Bell, T. G., Simó, R., Vallina, S. M., Ballabrera-Poy, J., Kettle, A. J., Dachs, J., Bopp, L., Saltzman, E. S., Stefels, J., Johnson, J. E., and Liss, P. S.: An updated climatology of surface dimethylsulfide concentrations and emission fluxes in the global ocean, *Global Biogeochemical Cycles*, 25, n/a–n/a, <https://doi.org/10.1029/2010GB003850>, 2011.
- Lannuzel, D., Wongpan, P., Hayashida, H., and Burke, G.: A data collation for climate-cooling gas dimethylsulphide in Antarctic snow, sea ice and underlying seawater, Ver. 1., <https://doi.org/10.26179/svwx-kt31>, 2024.
- Liss, P. S. and Merlivat, L.: Air-Sea Gas Exchange Rates: Introduction and Synthesis, in: *The Role of Air-Sea Exchange in Geochemical Cycling*, edited by Buat-Ménard, P., pp. 113–127, Springer Netherlands, Dordrecht, [https://doi.org/10.1007/978-94-009-4738-2\\_5](https://doi.org/10.1007/978-94-009-4738-2_5), 1986.
- 870 Mace, G. G., Benson, S., Sterner, E., Protat, A., Humphries, R., and Hallar, A. G.: The Association Between Cloud Droplet Number over the Summer Southern Ocean and Air Mass History, *Journal of Geophysical Research: Atmospheres*, 129, <https://doi.org/10.1029/2023JD040673>, 2024.
- Mallet, M. D., Cravigan, L. T., Milic, A., Alroe, J., Ristovski, Z. D., Ward, J., Keywood, M., Williams, L. R., Selleck, P., and Miljevic, B.: Composition, size and cloud condensation nuclei activity of biomass burning aerosol from northern Australian savannah fires, *Atmospheric Chemistry and Physics*, 17, 3605–3617, <https://doi.org/10.5194/acp-17-3605-2017>, 2017.
- 875 Mallet, M. D., Humphries, R. S., Fiddes, S. L., Alexander, S. P., Altieri, K., Angot, H., Anilkumar, N., Bartels-Rausch, T., Creamean, J., Dall’Osto, M., Dommergue, A., Frey, M., Henning, S., Lannuzel, D., Lapere, R., Mace, G. G., Mahajan, A. S., McFarquhar, G. M., Meiners, K. M., Miljevic, B., Peeken, I., Protat, A., Schmale, J., Steiner, N., Sellegri, K., Simó, R., Thomas, J. L., Willis, M. D., Winton, V. H. L., and Woodhouse, M. T.: Untangling the influence of Antarctic and Southern Ocean life on clouds, *Elementa: Science of the Anthropocene*, 11, <https://doi.org/10.1525/elementa.2022.00130>, 2023.
- 880 Mann, G. W., Carslaw, K. S., Spracklen, D. V., Ridley, D. A., Manktelow, P. T., Chipperfield, M. P., Pickering, S. J., and Johnson, C. E.: Description and evaluation of GLOMAP-mode: a modal global aerosol microphysics model for the UKCA composition-climate model, *Geosci. Model Dev*, 3, 519–551, <https://doi.org/10.5194/gmd-3-519-2010>, 2010.
- 885 Mann, G. W., Carslaw, K. S., Ridley, D. A., Spracklen, D. V., Pringle, K. J., Merikanto, J., Korhonen, H., Schwarz, J. P., Lee, L. A., Manktelow, P. T., Woodhouse, M. T., Schmidt, A., Breider, T. J., Emmerson, K. M., Reddington, C. L., Chipperfield, M. P., and Pickering, S. J.: Intercomparison of modal and sectional aerosol microphysics representations within the same 3-D global chemical transport model, *Atmospheric Chemistry and Physics*, 12, 4449–4476, <https://doi.org/10.5194/acp-12-4449-2012>, 2012.
- Marchand, R.: Macquarie Island Cloud and Radiation Experiment (MICRE) Field Campaign Report, Tech. rep., Atmospheric Radiation Measurement (ARM) Archive, Oak Ridge National Laboratory (ORNL), Oak Ridge, TN (US), <https://doi.org/10.2172/1602536>, 2020.
- 890 McCluskey, C. S., Hill, T. C. J., Malfatti, F., Sultana, C. M., Lee, C., Santander, M. V., Beall, C. M., Moore, K. A., Cornwell, G. C., Collins, D. B., Prather, K. A., Jayarathne, T., Stone, E. A., Azam, F., Kreidenweis, S. M., and DeMott, P. J.: A Dynamic Link between



- Ice Nucleating Particles Released in Nascent Sea Spray Aerosol and Oceanic Biological Activity during Two Mesocosm Experiments, *Journal of the Atmospheric Sciences*, 74, 151–166, <https://doi.org/10.1175/JAS-D-16-0087.1>, 2017.
- 895 McCluskey, C. S., Hill, T. C., Humphries, R. S., Rauker, A. M., Moreau, S., Stratton, P. G., Chambers, S. D., Williams, A. G., McRobert, I., Ward, J., Keywood, M. D., Harnwell, J., Ponsonby, W., Loh, Z. M., Krummel, P. B., Protat, A., Kreidenweis, S. M., and DeMott, P. J.: Observations of Ice Nucleating Particles Over Southern Ocean Waters, *Geophysical Research Letters*, 45, 989–11, <https://doi.org/10.1029/2018GL079981>, 2018.
- McCluskey, C. S., Gettelman, A., Bardeen, C. G., DeMott, P. J., Moore, K. A., Kreidenweis, S. M., Hill, T. C., Barry, K. R., Twohy, C. H., Toohey, D. W., Rainwater, B., Jensen, J. B., Reeves, J. M., Alexander, S. P., and McFarquhar, G. M.: Simulating Southern Ocean Aerosol and Ice Nucleating Particles in the Community Earth System Model Version 2, *Journal of Geophysical Research: Atmospheres*, 128, <https://doi.org/10.1029/2022JD036955>, 2023.
- 900 McCormick, R. A. and Ludwig, J. H.: Climate Modification by Atmospheric Aerosols, *Science*, 156, 1358–1359, <https://doi.org/10.1126/science.156.3780.1358>, 1967.
- McCoy, I. L., Bretherton, C. S., Wood, R., Twohy, C. H., Gettelman, A., Bardeen, C. G., and Toohey, D. W.: Influences of Recent Particle Formation on Southern Ocean Aerosol Variability and Low Cloud Properties, *Journal of Geophysical Research: Atmospheres*, 126, <https://doi.org/10.1029/2020JD033529>, 2021.
- 905 McFarquhar, G. M., Bretherton, C. S., Marchand, R., Protat, A., DeMott, P. J., Alexander, S. P., Roberts, G. C., Twohy, C. H., Toohey, D., Siems, S., Huang, Y., Wood, R., Rauber, R. M., Lasher-Trapp, S., Jensen, J., Stith, J. L., Mace, J., Um, J., Järvinen, E., Schnaiter, M., Gettelman, A., Sanchez, K. J., McCluskey, C. S., Russell, L. M., McCoy, I. L., Atlas, R. L., Bardeen, C. G., Moore, K. A., Hill, T. C. J., Humphries, R. S., Keywood, M. D., Ristovski, Z., Cravigan, L., Schofield, R., Fairall, C., Mallet, M. D., Kreidenweis, S. M., Rainwater, B., D'Alessandro, J., Wang, Y., Wu, W., Saliba, G., Levin, E. J. T., Ding, S., Lang, F., Truong, S. C. H., Wolff, C., Haggerty, J., Harvey, M. J., Klekociuk, A. R., and McDonald, A.: Observations of Clouds, Aerosols, Precipitation, and Surface Radiation over the Southern Ocean: An Overview of CAPRICORN, MARCUS, MICRE, and SOCRATES, *Bulletin of the American Meteorological Society*, 102, E894–E928, <https://doi.org/10.1175/BAMS-D-20-0132.1>, 2021.
- 915 Merikanto, J., Spracklen, D. V., Mann, G. W., Pickering, S. J., and Carslaw, K. S.: Impact of nucleation on global CCN, *Atmospheric Chemistry and Physics*, 9, 8601–8616, <https://doi.org/10.5194/acp-9-8601-2009>, 2009.
- Metzger, A., Verheggen, B., Dommen, J., Duplissy, J., Prevot, A. S. H., Weingartner, E., Riipinen, I., Kulmala, M., Spracklen, D. V., Carslaw, K. S., and Baltensperger, U.: Evidence for the role of organics in aerosol particle formation under atmospheric conditions., *Proceedings of the National Academy of Sciences of the United States of America*, 107, 6646–51, <https://doi.org/10.1073/pnas.0911330107>, 2010.
- 920 Modini, R. L., Ristovski, Z. D., Johnson, G. R., He, C., Surawski, N., Morawska, L., Suni, T., and Kulmala, M.: New particle formation and growth at a remote, sub-tropical coastal location, *Atmospheric Chemistry and Physics Discussions*, 9, 12 101–12 139, <https://doi.org/10.5194/acpd-9-12101-2009>, 2009.
- Mulcahy, J. P., Jones, C., Sellar, A., Johnson, B., Boutle, I. A., Jones, A., Andrews, T., Rumbold, S. T., Mollard, J., Bellouin, N., Johnson, C. E., Williams, K. D., Grosvenor, D. P., and McCoy, D. T.: Improved Aerosol Processes and Effective Radiative Forcing in HadGEM3 and UKESM1, *Journal of Advances in Modeling Earth Systems*, 10, 2786–2805, <https://doi.org/10.1029/2018MS001464>, 2018.
- 925 Oke, P. R., Griffin, D. A., Schiller, A., Matear, R. J., Fiedler, R., Mansbridge, J., Lenton, A., Cahill, M., Chamberlain, M. A., and Ridgway, K.: Evaluation of a near-global eddy-resolving ocean model, *Geoscientific Model Development*, 6, 591–615, <https://doi.org/10.5194/gmd-6-591-2013>, 2013.



- Paulot, F., Paynter, D., Winton, M., Ginoux, P., Zhao, M., and Horowitz, L. W.: Revisiting the Impact of Sea Salt on Climate Sensitivity, *Geophysical Research Letters*, 47, <https://doi.org/10.1029/2019GL085601>, 2020.
- 930 Petters, M. D. and Kreidenweis, S. M.: A single parameter representation of hygroscopic growth and cloud condensation nucleus activity, *Atmospheric Chemistry and Physics*, 7, 1961–1971, <https://doi.org/10.5194/acp-7-1961-2007>, 2007.
- Pincus, R. and Baker, M. B.: Effect of precipitation on the albedo susceptibility of clouds in the marine boundary layer, *Nature*, 372, 250–252, <https://doi.org/10.1038/372250a0>, 1994.
- 935 Prather, K. A., Bertram, T. H., Grassian, V. H., Deane, G. B., Stokes, M. D., DeMott, P. J., Aluwihare, L. I., Palenik, B. P., Azam, F., Seinfeld, J. H., Moffet, R. C., Molina, M. J., Cappa, C. D., Geiger, F. M., Roberts, G. C., Russell, L. M., Ault, A. P., Baltrusaitis, J., Collins, D. B., Corrigan, C. E., Cuadra-Rodriguez, L. A., Ebben, C. J., Forestieri, S. D., Guasco, T. L., Hersey, S. P., Kim, M. J., Lambert, W. F., Modini, R. L., Mui, W., Pedler, B. E., Ruppel, M. J., Ryder, O. S., Schoepp, N. G., Sullivan, R. C., and Zhao, D.: Bringing the ocean into the laboratory to probe the chemical complexity of sea spray aerosol, *Proceedings of the National Academy of Sciences of the United States*
- 940 *of America*, 110, 7550–7555, <https://doi.org/10.1073/pnas.1300262110>, 2013.
- Protat, A.: RV Investigator BOM Atmospheric Data Overview (2016 onwards), <https://doi.org/https://doi.org/10.25919/5f688fcc97166>, 2020.
- Protat, A., Schulz, E., Rikus, L., Sun, Z., Xiao, Y., and Keywood, M. D.: Shipborne observations of the radiative effect of Southern Ocean clouds, *Journal of Geophysical Research: Atmospheres*, 122, 318–328, <https://doi.org/10.1002/2016JD026061>, 2017.
- Quinn, P. K. and Bates, T. S.: The case against climate regulation via oceanic phytoplankton sulphur emissions, *Nature*, 480, 51–56, <https://doi.org/10.1038/nature10580>, 2011.
- 945 Quinn, P. K., Collins, D. B., Grassian, V. H., Prather, K. A., and Bates, T. S.: Chemistry and Related Properties of Freshly Emitted Sea Spray Aerosol, <https://doi.org/10.1021/cr500713g>, 2015.
- Regayre, L. A., Schmale, J., Johnson, J. S., Tatzelt, C., Baccarini, A., Henning, S., Yoshioka, M., Stratmann, F., Gysel-Beer, M., Grosvenor, D. P., and Carslaw, K. S.: The value of remote marine aerosol measurements for constraining radiative forcing uncertainty, *Atmospheric*
- 950 *Chemistry and Physics*, 20, 10 063–10 072, <https://doi.org/10.5194/acp-20-10063-2020>, 2020.
- Revell, L. E., Kremser, S., Hartery, S., Harvey, M., Mulcahy, J. P., Williams, J., Morgenstern, O., McDonald, A. J., Varma, V., Bird, L., and Schuddeboom, A.: The sensitivity of Southern Ocean aerosols and cloud microphysics to sea spray and sulfate aerosol production in the HadGEM3-GA7.1 chemistry-climate model, *Atmospheric Chemistry and Physics*, 19, 15 447–15 466, <https://doi.org/10.5194/acp-19-15447-2019>, 2019.
- 955 Revell, L. E., Wotherspoon, N. E., Jones, O. J., Bhatti, Y. A., Williams, J. H. T., Mackie, S. L., and Mulcahy, J. P.: Atmosphere-Ocean Feedback From Wind-Driven Sea Spray Aerosol Production, *Geophysical Research Letters*, 48, <https://doi.org/10.1029/2020GL091900>, 2021.
- Rodríguez-Ros, P., Galí, M., Cortés, P., Robinson, C. M., Antoine, D., Wohl, C., Yang, M. X., and Simó, R.: Remote Sensing Retrieval of Isoprene Concentrations in the Southern Ocean, *Geophysical Research Letters*, 47, <https://doi.org/10.1029/2020GL087888>, 2020.
- 960 Russell, L. M., Moore, R. H., Burrows, S. M., and Quinn, P. K.: Ocean flux of salt, sulfate, and organic components to atmospheric aerosol, *Earth-Science Reviews*, 239, 104 364, <https://doi.org/10.1016/j.earscirev.2023.104364>, 2023.
- Schmale, J., Baccarini, A., Thurnherr, I., Henning, S., Efraim, A., Regayre, L., Bolas, C., Hartmann, M., Welti, A., Lehtipalo, K., Aemisegger, F., Tatzelt, C., Landwehr, S., Modini, R. L., Tummon, F., Johnson, J. S., Harris, N., Schnaiter, M., Toffoli, A., Derkani, M., Bukowiecki, N., Stratmann, F., Dommen, J., Sperger, U. B., Wernli, H., Rosenfeld, D., Gysel-Beer, M., and Carslaw, K. S.: Overview of the antarctic circumnavigation expedition: Study of preindustrial-like aerosols and their climate effects (ACE-SPACE), *Bulletin of the American*
- 965 *Meteorological Society*, 100, 2260–2283, <https://doi.org/10.1175/BAMS-D-18-0187.1>, 2019.



- Schofield, R. and Ryan, R.: Observations collected between 18th October 2018 and 29th March 2019 aboard Aurora Australis by AIRBOX and associated instruments, Ver. 1, <https://doi.org/http://dx.doi.org/doi:10.26179/5e546f452145d>, 2021.
- Schuddeboom, A. J. and McDonald, A. J.: The Southern Ocean Radiative Bias, Cloud Compensating Errors, and Equilibrium Climate Sensitivity in CMIP6 Models, *Journal of Geophysical Research: Atmospheres*, 126, <https://doi.org/10.1029/2021JD035310>, 2021.
- 970 Sellegri, K., Barthelmeß, T., Trueblood, J., Cristi, A., Freney, E., Rose, C., Barr, N., Harvey, M., Safi, K., Deppeler, S., Thompson, K., Dillon, W., Engel, A., and Law, C.: Quantified effect of seawater biogeochemistry on the temperature dependence of sea spray aerosol fluxes, *Atmospheric Chemistry and Physics*, 23, 12 949–12 964, <https://doi.org/10.5194/acp-23-12949-2023>, 2023.
- Simmons, J. B., Humphries, R. S., Wilson, S. R., Chambers, S. D., Williams, A. G., Griffiths, A. D., McRobert, I. M., Ward, J. P., Keywood, M. D., and Gribben, S.: Summer aerosol measurements over the East Antarctic seasonal ice zone, *Atmospheric Chemistry and Physics*, 21, 9497–9513, <https://doi.org/10.5194/acp-21-9497-2021>, 2021.
- 975 Trevena, A. and Jones, G.: DMS flux over the Antarctic sea ice zone, *Marine Chemistry*, 134-135, 47–58, <https://doi.org/10.1016/j.marchem.2012.03.001>, 2012.
- Twomey, S.: Pollution and the Planetary Albedo, *Atmospheric Environment*, 8, 1251–1256, 1974.
- 980 Uin, J., Aiken, A. C., Dubey, M. K., Kuang, C., Pekour, M., Salwen, C., Sedlacek, A. J., Senum, G., Smith, S., Wang, J., Watson, T. B., and Springston, S. R.: Atmospheric radiation measurement (ARM) aerosol observing systems (AOS) for surface-based in situ atmospheric aerosol and trace gas measurements, *Journal of Atmospheric and Oceanic Technology*, 36, 2429–2447, <https://doi.org/10.1175/JTECH-D-19-0077.1>, 2019.
- Van Marle, M. J., Kloster, S., Magi, B. I., Marlon, J. R., Daniau, A. L., Field, R. D., Arneeth, A., Forrest, M., Hantson, S., Kehrwald, N. M., Knorr, W., Lasslop, G., Li, F., Mangeon, S., Yue, C., Kaiser, J. W., and Van Der Werf, G. R.: Historic global biomass burning emissions for CMIP6 (BB4CMIP) based on merging satellite observations with proxies and fire models (1750-2015), <https://doi.org/10.5194/gmd-10-3329-2017>, 2017.
- 985 Venugopal, A. U., Bhatti, Y. A., Morgenstern, O., Williams, J., Edkins, N., Hardacre, C., Jones, A., and Revell, L. E.: Constraining the uncertainty associated with sea salt aerosol parameterizations in global models using nudged UKESM1-AMIP simulations, *JRR: Atmospheres* [preprint], in review, 2024.
- Vergara-Temprado, J., Miltenberger, A. K., Furtado, K., Grosvenor, D. P., Shipway, B. J., Hill, A. A., Wilkinson, J. M., Field, P. R., Murray, B. J., and Carslaw, K. S.: Strong control of Southern Ocean cloud reflectivity by ice-nucleating particles, *Proceedings of the National Academy of Sciences of the United States of America*, 115, 2687–2692, <https://doi.org/10.1073/pnas.1721627115>, 2018.
- Vignon, E., Alexander, S. P., DeMott, P. J., Sotiropoulou, G., Gerber, F., Hill, T. C. J., Marchand, R., Nenes, A., and Berne, A.: Challenging and Improving the Simulation of Mid-Level Mixed-Phase Clouds Over the High-Latitude Southern Ocean, *Journal of Geophysical Research: Atmospheres*, 126, <https://doi.org/10.1029/2020JD033490>, 2021.
- 995 Vlahos, P. and Monahan, E. C.: A generalized model for the air-sea transfer of dimethyl sulfide at high wind speeds, *Geophysical Research Letters*, 36, L21 605, <https://doi.org/10.1029/2009GL040695>, 2009.
- Walters, D., Baran, A. J., Boutle, I., Brooks, M., Earnshaw, P., Edwards, J., Furtado, K., Hill, P., Lock, A., Manners, J., Morcrette, C., Mulcahy, J., Sanchez, C., Smith, C., Stratton, R., Tennant, W., Tomassini, L., Van Weverberg, K., Vosper, S., Willett, M., Browse, J., Bushell, A., Carslaw, K., Dalvi, M., Essery, R., Gedney, N., Hardiman, S., Johnson, B., Johnson, C., Jones, A., Jones, C., Mann, G., Milton, S., Rumbold, H., Sellar, A., Ujiie, M., Whitall, M., Williams, K., and Zerroukat, M.: The Met Office Unified Model Global Atmosphere 7.0/7.1 and JULES Global Land 7.0 configurations, *Geoscientific Model Development*, 12, 1909–1963, <https://doi.org/10.5194/gmd-12-1909-2019>, 2019.
- 1000



- 1005 Wang, W. L., Song, G., Primeau, F., Saltzman, E. S., Bell, T. G., and Moore, K. K.: Global ocean dimethyl sulfide climatology estimated from observations and an artificial neural network, *Biogeosciences*, 17, 5335–5354, <https://doi.org/10.5194/bg-17-5335-2020>, 2020.
- Watson-Parris, D. and Smith, C. J.: Large uncertainty in future warming due to aerosol forcing, *Nature Climate Change*, 12, 1111–1113, <https://doi.org/10.1038/s41558-022-01516-0>, 2022.
- Webb, A. L., van Leeuwe, M. A., den Os, D., Meredith, M. P., J. Venables, H., and Stefels, J.: Extreme spikes in DMS flux double estimates of biogenic sulfur export from the Antarctic coastal zone to the atmosphere, *Scientific Reports*, 9, <https://doi.org/10.1038/s41598-019-38714-4>, 2019.
- 1010 Woodward, S.: Modeling the atmospheric life cycle and radiative impact of mineral dust in the Hadley Centre climate model, *Journal of Geophysical Research: Atmospheres*, 106, 18 155–18 166, <https://doi.org/10.1029/2000JD900795>, 2001.
- World Meteorological Organization (WMO): WMO/GAW Aerosol Measurement Procedures, Guidelines and Recommendations, WMO, Geneva, 2nd edition edn., <https://library.wmo.int/idurl/4/55277>, 2016.
- 1015 Zelinka, M. D., Myers, T. A., McCoy, D. T., Po-Chedley, S., Caldwell, P. M., Ceppi, P., Klein, S. A., and Taylor, K. E.: Causes of Higher Climate Sensitivity in CMIP6 Models, *Geophysical Research Letters*, 47, 1–12, <https://doi.org/10.1029/2019GL085782>, 2020.
- Zhou, S., Chen, Y., Huang, S., Gong, X., Yang, G., Zhang, H., Herrmann, H., Wiedensohler, A., Poulain, L., Zhang, Y., Wang, F., Xu, Z., and Yan, K.: A 20-year (1998–2017) global sea surface dimethyl sulfide gridded dataset with daily resolution, *Earth System Science Data*, 16, 4267–4290, <https://doi.org/10.5194/essd-16-4267-2024>, 2024.
- 1020